Multi-Cyclic and Isotopically Diverse Silicic Magma Generation in an Arc Volcano: Gorely Eruptive Center, Kamchatka, Russia

A. SELIGMAN[1]*, I. BINDEMAN[1], B. JICHA[2], B. ELLIS[3], V. PONOMAREVA[4] AND V. LEONOV[4]

[1]GEOLOGICAL SCIENCES, 1272 UNIVERSITY OF OREGON, EUGENE, OR 97403, USA

[2]DEPARTMENT OF GEOSCIENCE, UNIVERSITY OF WISCONSIN–MADISON, MADISON, WI 53706, USA

[3]INSTITUTE OF GEOCHEMISTRY AND PETROLOGY, DEPARTMENT OF EARTH SCIENCES, ETH ZURICH, SWITZERLAND

[4]INSTITUTE OF VOLCANOLOGY AND SEISMOLOGY, PETROPAVLOVSK-KAMCHATSKY, RUSSIA

The Kamchatka Peninsula is home to some of the most frequent and prolific subduction-related volcanic activity in the world, with the largest number of caldera-forming eruptions per length of the volcanic arc. Among those, Gorely volcano has a topographically prominent Late Pleistocene caldera (13 km × 12 km, estimated to have produced >100 km³ of magma), which is now almost completely filled by a central cone. We report new $^{40}Ar/^{39}Ar$ ages and geochemical and isotopic data for newly recognized Mid-Pleistocene ignimbrite units of large but unknown volume sourced from the Gorely eruptive center, most of which were deposited in marginal glacial conditions. These ignimbrites have crystallinities of 9–24% and most are quartz-, amphibole-, and zircon-undersaturated. Additionally, we studied 32 eruptive units, including stratigraphically constrained Holocene tephra, and pre- and post-caldera lava sequences, to understand the petrogenetic and temporal evolution of this long-lived, multi-cyclic, arc volcano. Material erupted prior to the formation of the modern Gorely edifice, including the voluminous ignimbrites and eruptions of the 'pra-Gorely' stage, consist primarily of dacite and andesite, whereas sequences of the modern Gorely edifice are represented by basalt to basaltic andesite. MELTS and EC-AFC modeling shows that it is possible to obtain silicic compositions near those of the evolved ignimbrite compositions through 60–75% fractional crystallization at 1 kbar and nickel–nickel oxide (NNO) oxygen fugacity. However, our newly compiled major and trace element data for Gorely yield two separate bimodal peaks in a SiO_2–frequency diagram, showing a prominent Daly Gap, with a deficiency in andesite. Trace element concentrations define two separate trends, one for more silicic and another for more mafic sequences. Additionally, $\delta^{18}O_{melt}$ values reconstructed from coexisting plagioclase and clinopyroxene phenocrysts range from a low value of 4·85‰ to a normal value of 6·22‰. The low $\delta^{18}O$ values range throughout the known lifespan of Gorely, with the lowest value being from the first known ignimbrite to erupt, indicating episodic but temporally decreasing crustal assimilation of previously hydrothermally altered material. $^{87}Sr/^{86}Sr$ and $^{143}Nd/^{144}Nd$ ratios show wide ranges from 0·70328 to 0·70351 and from 0·51303 to 0·51309 respectively, also suggesting incorporation of surrounding crust, although there are less clear trends throughout the lifespan of Gorely. The combination of light and diverse $\delta^{18}O$ values with elevated $^{87}Sr/^{86}Sr$ and low $^{143}Nd/^{144}Nd$ ratios suggests contamination by older and isotopically diverse, low-$\delta^{18}O$ country-rocks, such as the neighboring 11 Ma Akhomten granitic massif, which shows ranges in $\delta^{18}O$, $^{87}Sr/^{86}Sr$, and $^{144}Nd/^{143}Nd$ values overlapping with the Gorely magmas. In addition, the presence of glomerocrysts and mafic enclaves in the majority of Gorely dacites indicates a period of crystal settling and subsequent intrusion of hot, primitive basalt that probably triggered eruption. Finally, elevated Nb concentrations relative to other Kamchatkan volcanoes suggest that Gorely magmas may involve an enriched component, probably caused by delamination of a lower crustal root. Our results argue for an incremental view of silicic magma generation at so-called 'long-term eruptive centers', in Kamchatka and worldwide, consisting of alternating episodes of magmatic and hydrothermal activity, and glacial advances and retreats. We demonstrate that large-volume, isotopically distinct, silicic

* Corresponding author. E-mail: seligman@uoregon.edu

magma can be generated rapidly between cone-building phases of volcanic activity through a combination of fractional crystallization, assimilation of older country rocks, and shallow assimilation of hydrothermally altered but otherwise petrochemically similar older intracaldera tuffs and intrusions. These transient shallow silicic magma chambers empty nearly completely in ignimbrite-forming eruptions after 10^3–10^5 years of assembly, partially triggered by glacial surface dynamics.

KEY WORDS: *EC-AFC; ignimbrite; isotope; Kamchatka; long-term eruptive center*

INTRODUCTION

Origin of silicic magmas in arc crust

A long-standing question in igneous petrology is how silicic magmas are formed in subduction-related settings and their relation to the formation and recycling of continental crust, as well as its compositional (mafic–silicic) stratification (Rudnick & Fountain, 1995). Mafic magmatism at subduction zones is obviously the initial step to producing more silicic compositions through either fractional crystallization (e.g. Gill, 1981; Grove & Kinzler, 1986; Musselwhite *et al.*, 1989; Rogers & Hawkesworth, 1989; Müntener *et al.*, 2001; Grove *et al.*, 2002, 2003), crustal assimilation (Bohrson & Spera, 2001; Spera & Bohrson, 2001), or partial melting of pre-existing silicic crust (e.g. Smith & Leeman, 1987; Atherton & Petford, 1993; Tepper *et al.*, 1993; Rapp & Watson, 1995; Petford & Atherton, 1996; Chappell & White, 2001; Izbekov *et al.*, 2004*b*), previously erupted volcanic rocks (Simakin & Bindeman, 2012), or of more mafic crust and cumulates stored in the magma chamber following prior eruptions (e.g. Heath *et al.*, 1998; Dungan & Davidson, 2004). However, these processes probably occur simultaneously, as predicted by heat- and mass-balance calculations (Dufek & Bergantz, 2005; Annen *et al.*, 2006) and models such as energy constrained assimilation–fractional crystallization (EC-AFC; Bohrson & Spera, 2001; Spera & Bohrson, 2001), and probably include magma–magma and magma–cumulate mixing, which leads to long-term modification, assimilation, storage, and hybridization (MASH; Hildreth & Moorbath, 1988; Annen *et al.*, 2006), and upward sequestration of silicic components via recycling (e.g. Simakin & Bindeman, 2012). This study provides a detailed look at the processes responsible for the formation of evolved magmas extruded from the Gorely eruptive center of the Kamchatkan volcanic arc (Fig. 1) by using the tools of isotope and trace element geochemistry, and crystallization modeling.

Geological background and overview of the Gorely eruptive history

The Kamchatka Peninsula, located in the NW Pacific (Fig. 1), has some of the most frequent and prolific subduction-related volcanic activity on Earth, including the largest number of calderas relative to the size of the volcanic arc, owing to fast convergence (Siebert & Simkin, 2002; Hughes & Mahood, 2008; Bindeman *et al.*, 2010). These volcanoes account for over 16% of global on-land volcanic ejecta, and discharge *c.* 240×10^6 tons of material annually (Erlich & Gorshkov, 1979). Most of the current volcanic activity is concentrated in the Eastern Volcanic Belt, which stretches from northern to southern Kamchatka as a result of subduction of the 80–100 Ma Pacific Plate beneath the Kamchatkan Peninsula at *c.* 7–8 cm a^{-1}, with an average slab dip of *c.* 55° (Gorbatov *et al.*, 1997, 1999) (Fig. 1). One of these typical caldera-forming volcanoes, Gorely, is located in the southern part of the peninsula in the Eastern Volcanic Belt (Fig. 1).

The Gorely volcanic center has been characterized by a series of explosive and cone-building eruptions throughout its evolution, creating a complex edifice with a currently active summit crater (Fig. 2). Topographically, this eruptive center consists of a large (13 km × 12 km) caldera, which encloses the currently active basaltic to andesitic Gorely composite volcano (Fig. 2). Several thick, welded and non-welded tuffs exposed in the vicinity of the present caldera suggest the occurrence of more than one caldera-forming eruption from this center, so that the modern caldera might in fact represent the latest of a suite of nested calderas. The most recent caldera, with an estimated eruptive volume exceeding 100 km^3, based on the caldera size of 12 km × 13 km (Selyangin, 2006), is believed to have formed around 38 ka based on dates for a distal tephra deposit (Braitseva *et al.*, 1995; all the dates for the last ∼40 kyr are calibrated ^{14}C). Several attempts to determine the age of the youngest welded tuff unit in the area by using ^{40}Ar/^{39}Ar geochronology failed owing to the predominance of atmospheric Ar. Traditionally, all the welded tuffs around the Gorely caldera (Fig. 2) were assumed to be associated with the most recent caldera-forming eruption (Selyangin & Ponomareva, 1999). A recent dating effort, however, has revealed that some of these welded tuffs may belong to far older mid-Pleistocene (361 ka) eruptions (Bindeman *et al.*, 2010). The youngest welded tuff, in places, is overlain by a dacitic pumice, which may represent the product of the most recent caldera-forming eruption (*c.* ∼38 ka) and resulting depression of the western part of the caldera (Selyangin & Ponomareva, 1999). Shortly after the cycle of cataclysmic eruptions, a series of smaller eruptions along the caldera rim created basaltic andesite cinder cones and dacite extrusions. The modern intra-caldera volcanic edifice started to form in late Pleistocene times (Selyangin & Ponomareva, 1999) and comprises three merged cones, of which the first two formed under glaciers (Fig. 2). Gorely 1, the first cone to form, is composed of 14 km^3 of primarily basalt and basaltic andesite. Gorely 2 began to form in the early
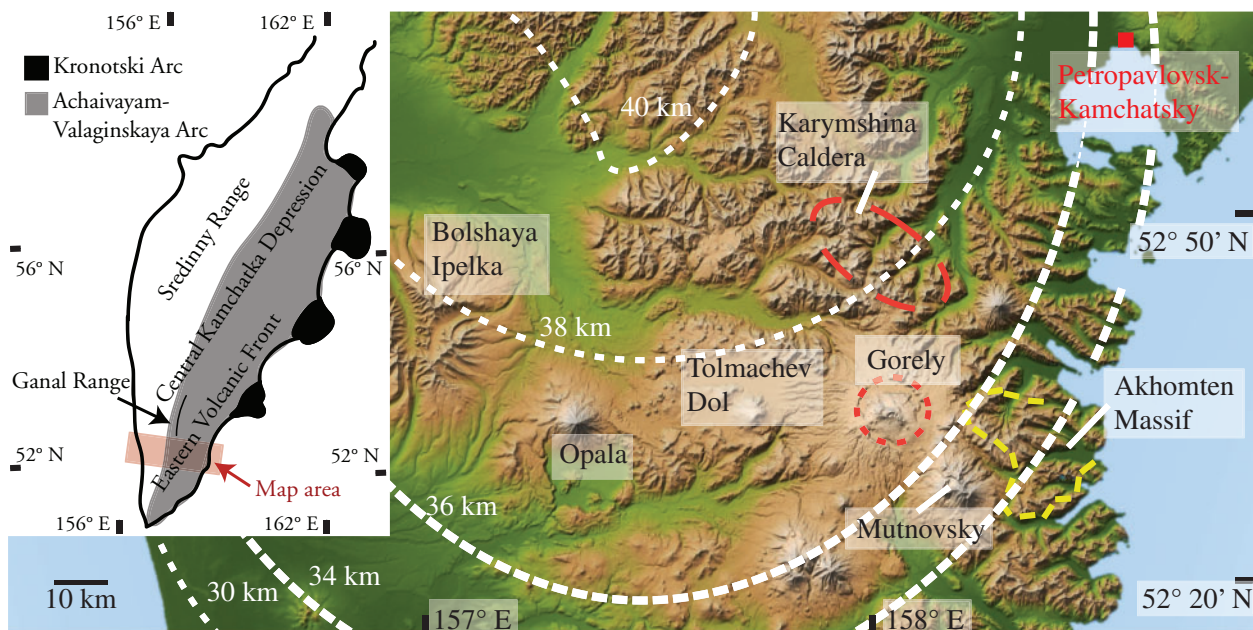
Fig. 1. Digital elevation map of south–central Kamchatka showing Gorely volcano and other nearby volcanic centers. Red dashed lines indicate the approximate boundary of the 1·8 Ma Karymshina and 0·3–0·038 Ma Gorely calderas. Outcrops of the 11 Ma Akhomten Granite Massif are outlined in yellow. White dashed lines indicate the thickness of the Kamchatkan crust (from Baboshina *et al.*, 2000). Inset shows the location of the Sredinny Range, the Central Kamchatka Depression, the Eastern Volcanic Front, The Ganal Range, the Kronotski Arc, and the Achaivayam–Valaginskaya Arc for reference [Bindeman *et al.* (2002) and references therein].

Holocene at the eastern edge of the crater of Gorely 1, and is still active today, erupting primarily basalt to basaltic andesite. Gorely 3 is the smallest of the three merged cones (2 km^3) and formed at the southeastern flank of Gorely 2. Gorely 3 is composed primarily of basaltic to andesitic lavas and pyroclastic material. In addition to the summit craters, there are also numerous fissures along the flanks of Gorely, which began developing prior to the Holocene, and continue to erupt episodically today (Kirsanov & Melekestev, 1991; Chashchin, 1999; Selyangin & Ponomareva, 1999; Selyangin, 2006). The youngest lava eruptions occurred along an arcuate fissure in AD 1737 (Selyangin, 2006), and intermittent volcanic activity continues today, accompanied by nearly continual release of steam and gas.

Tectonic history and crustal structure of the Eastern Volcanic Front

Previous research on the tectonic history of Kamchatka has provided significant insight into the initiation of volcanic activity in the region, the origin of the *c.* 37 km thick crust underlying the Gorely eruptive center, and the origin of the crust of the Eastern Volcanic Front (Balesta, 1991; Kraus & Scotese, 1993; Gordeev *et al.*, 2001; Bindeman *et al.*, 2002; Soloviev *et al.*, 2002a, 2002b; Konstantinovskaya, 2003; Lander & Shapiro, 2007; Scholl, 2007; Hourigan *et al.*, 2009). Prior to ~10 Ma, subduction

occurred below the Sredinny Range, 150 km west of the modern volcanic front (Lander & Shapiro, 2007) (Fig. 1). Accretion of the Kronotski arc between 10 and 7 Ma to eastern Kamchatka (Lander & Shapiro, 2007) caused subduction to jump to the east. The Eastern Volcanic Belt, in which the Gorely eruptive center is located, was established at around 5 Ma, owing to steeper subduction and migration of the trench to the east. Because the Kronotski terrane collided with Kamchatka at an oblique angle, collision began in the south and migrated north through time (Lander & Shapiro, 2007). Outcrops of the Miocene Akhomten Granite Massif are exposed to the east of Gorely, suggesting that similar crust may extend beneath the volcano (Figs 1–3). It is also possible that the crust underlying Gorely may include crust from the Achaivayam–Valaginsky Arc, which accreted at 45–50 Ma; this is also known as the Olutorsky Arc (Soloviev *et al.*, 2002a, 2002b; Konstantinovskaya, 2003; Hourigan *et al.*, 2009), and is similar to exposures at Ganal Range (e.g. Bindeman *et al.*, 2002), or metamorphosed accretionary sediments trapped between the Achaivayam–Valaginsky Arc and the Ganal Range (Soloviev *et al.*, 2002b; Konstantinovskaya, 2003) (Fig. 1).

Goals of this study

This study focuses on the processes responsible for the formation of silicic magmas in arc crust at a typical multi-caldera, 'long-lived' eruptive center represented by Gorely.
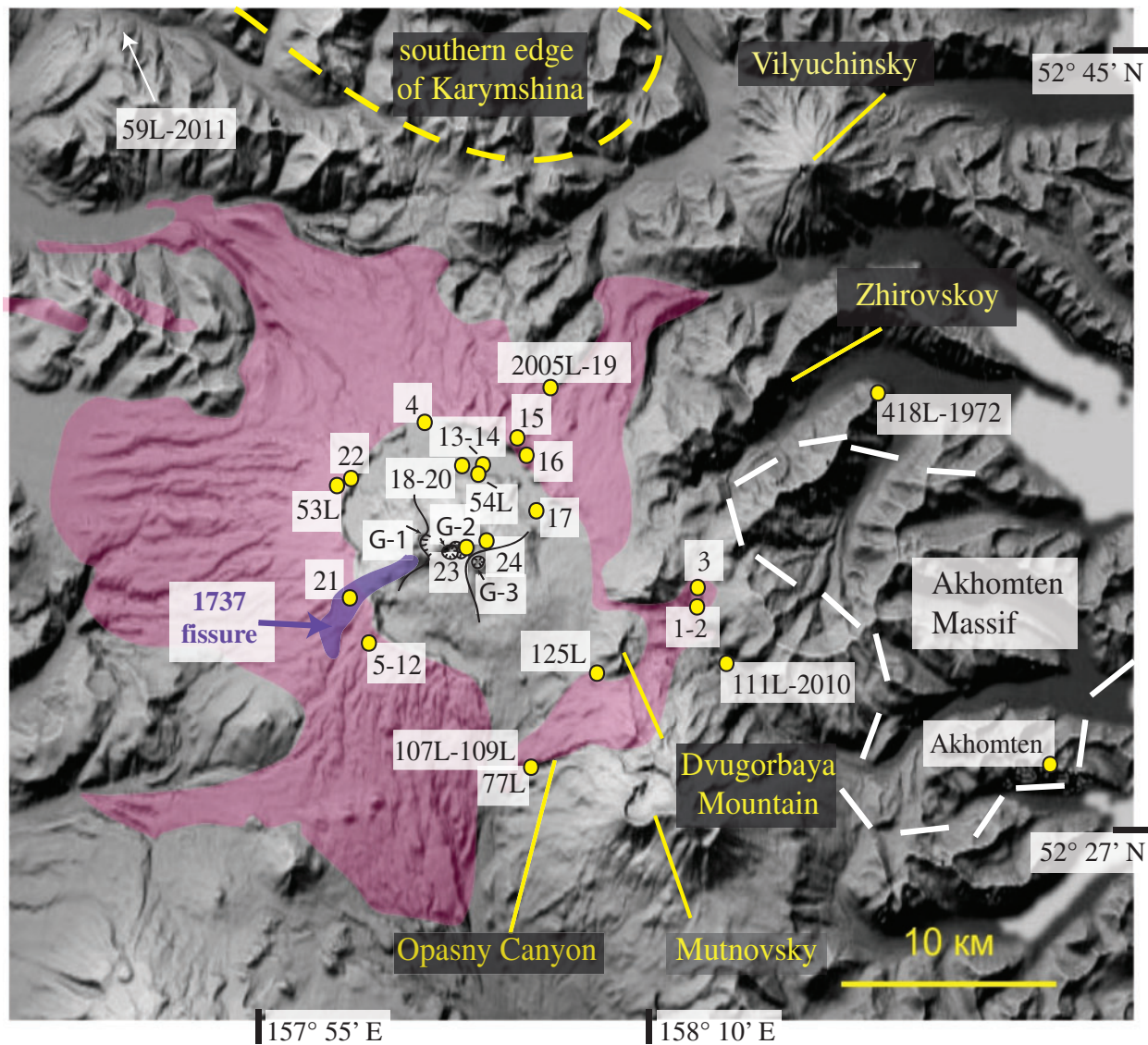
Fig. 2. Digital elevation map of Gorely volcano and its surrounding caldera, showing the extent of the ignimbrites and pumice, which are described in this study (shaded in pink), and the location of the studied samples. The sample names have been abbreviated (e.g.'11G-3' is written as '3', and '77L-l44' is written as '77L'). The locations of Opasny Canyon, Mutnovsky volcano, Zhirovskoy volcano, Dvugorbaya Mountain, and Vilyuchinsky volcano are indicated. White dashed lines denote outcrops of the Akhomten Massif, and yellow dashed lines denote the extent of the southern edge of the Karymshina caldera. G-l, G-2, and G-3 refer to the Gorely-l, Gorely-2, and Gorely-3 cones, respectively.

In an attempt to determine these processes we use $^{87}Sr/^{86}Sr$, $^{144}Nd/^{143}Nd$, and $\delta^{18}O$ isotopic data in addition to major and trace element compositions, MELTS and EC-AFC modeling, $^{40}Ar/^{39}Ar$ geochronology, pyroxene and plagioclase chemistry, and thin section petrography. Detailed isotopic work allows us to assess the relative roles of fractional crystallization and crustal assimilation, and to recognize the importance of crustal recycling, even in this setting where the underlying crust is relatively young (Eocene–Quaternary) and petrochemically similar. This situation is typical of many volcanic arcs built on recently accreted terranes. We also address whether isotopically

distinct ignimbrites are produced from a large, single, long-lived magma body or multiple smaller magma bodies beneath the Gorely eruptive center, the likely time-scales of these processes, and how they relate to glaciations that shaped the area.

METHODS

Samples from this study (Figs 2 and 4, Supplementary Data Figs Al and A2; supplementary material is available for downloading at http://www.petrology.oxfordjournals.org) and Table 1 include a stratigraphic sequence of
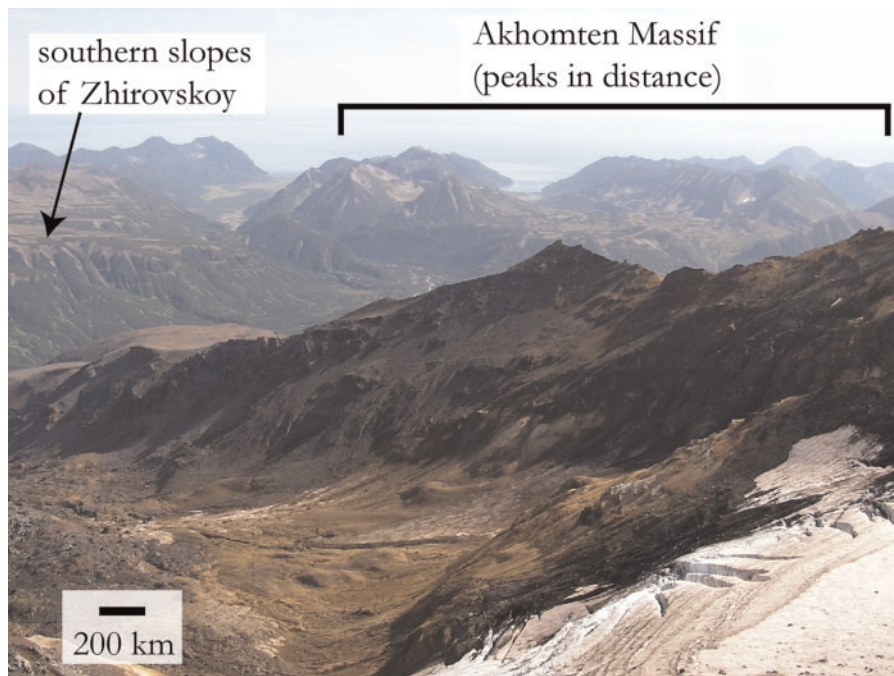
Fig. 3. Image looking NE from Mutnovsky volcano, showing the southern slopes of Zhirovskoy to the north and the Akhomten Massif in the background.

tephrochronologically dated (Supplementary Data: Fig. A1) Holocene (post-glacial) tephra collected from trenches near road cuts and river drainages, lavas collected from both 'pra-Gorely' ['pra-Gorely' is the term typically used for the older Gorely cone ($\sim$0·7 Ma) that was destroyed during a series of caldera-forming eruptions (Selyangin, 2006)] and modern Gorely, and multiple ignimbrites. Ages were determined for tephra units based on stratigraphic order and known ages of regional tephra markers present in the sections (Supplementary Data Fig. A1). These marker layers include KO (Kurile lake caldera, $\sim$8·4 ka), KS_2 (Ksudach caldera, $\sim$6·85 ka), KS_1 (Ksudach caldera, $\sim$1·75 ka), OP (Opala, 1·4 ka), and $KSht_3$ (Stübel Cone, Ksudach center AD 1907) (Selyangin & Ponomareva, 1999). Lavas collected for this study were assigned an age based on their known period of eruption (i.e. modern Gorely or pra-Gorely), historical dates, position relative to dated regional tephra, and reflected on the geological map of Selyangin (2006). One ignimbrite sample was collected near Gorely volcano, four older ignimbrite units were collected from Opasny (Dangerous) Canyon (Supplementary Data: Fig. A2), and one ignimbrite unit was collected near Dvugorbaya Mountain (Fig. 2; Table 1).

Samples were analyzed for $\delta^{18}O$ at the stable isotope laboratory of the University of Oregon. Single plagioclase and pyroxene grains as well as whole-rock fragments were picked from each sample using a binocular microscope, with most weights ranging from 1 to 2 mg. Grains were

selected from a 0·5–1 mm size fraction and grains lacking melt or crystal inclusions were selected preferentially. Samples were analyzed using CO_2-laser fluorination (e.g. Bindeman, 2008) with Gore Mt. Garnet ($\delta^{18}O$ of 5·75‰) as a standard and using BrF_5 reagent. The desired gas was acquired through a series of steps involving multiple LN_2 cryogenic traps that caused the BrF_5 reaction products to be frozen in a mercury diffusion pump as a getter for F_2 gas, leaving pure O_2 as an end result, which was then converted to CO_2 in a small platinum–graphite converter. After this step, the yield was measured as a means to determine any sample loss, and the CO_2 gas was analyzed on a MAT 253 mass spectrometer for the isotopic ratio of $^{18}O/^{16}O$.

Whole-rock major and trace elements were determined by X-ray fluorescence (XRF) using standard methods in the GeoAnalytical Lab at Washington State University as described by Johnson *et al.* (1999). Doubly fused, low dilution beads were used to determine the major elements and a typical suite of trace elements. Analyses were carried using a ThermoARL Advant'XP+sequential XRF spectrometer, with major elements reported as oxide weight per cent (anhydrous) and trace elements reported in parts per million.

The $^{87}Sr/^{86}Sr$ and $^{143}Nd/^{144}Nd$ isotope compositions of crushed whole-rock powders were determined by thermal ionization mass spectrometry (TIMS) at New Mexico State University. For these analyses, the freshest fragment of rock without any lithic fragments was picked from each
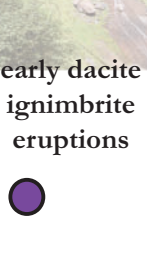
modern Gorely basalt-basaltic andesite cone-building stage ◆	**18th century fissure eruption (11G-21)**
	11G-12 (~0.8 ka tephra)
	11G-23 (~1.5 ka lava)
	~2 ka lavas (11G-24, 11G-4, 07L-54)
	11G-20 (~4 ka tephra)
	11G-19 (~5 ka tephra)
	~7 ka lavas and tephras (11G-18, 11G-17, 11G-14, 11G-13, 11G-7)
	~8 ka tephras (11G-10, 11G-9, 11G-8)
	lava of early monogenetic cone (~20 ka; 11G-5)
●	**late dacite ignimbrite eruption (~38 ka) (77L-144, 11G-3a/b, 07L-53)**
early dacite ignimbrite eruptions ●	**gap in dated material**
	109L-2010 (227±19 ka; $^{40}Ar/^{39}Ar$)
	125L-2000 (~227 ka)
	11G-1/2 (~300 ka)
	107L-2010 (332±6 ka; $^{40}Ar/^{39}Ar$)
	2005L-19 (361±8 ka; $^{40}Ar/^{39}Ar$) (Bindeman et al., 2010)
▲	**pra-Gorely dacite lavas (~700 ka) (11G-6, 11G-15, 11G-16)**
	Zhirovskoy basalt-andesite lava flows (0.7–0.8 Ma) (Sheimovich & Karpenko, 1996)
□	**Karymshina rhyolite Ignimbrites (~1.8 Ma) (Bindeman et al., 2010)**
✕	**nearby 4 Ma Qtz-biotite rhyolite Tuffs (111L-2010, 418L-1972, 59L-11)**
✚	**Akhomten Granite Massif (89L-19; 11.2 Ma; U-Pb)**
	Achaivayam-Valaginsky Arc (45-50 Ma) (Soloviev et al., 2002a, 2002b; Hourigan et al., 2009; Konstantinovskaya, 2003)

Fig. 4. Section illustrating the volcanic stratigraphy below Gorely volcano. Symbols and colors for each layer, where appropriate, are the same as those used in subsequent figures. Methods used for the ages reported in this section are also listed in Table 1. The image behind the modern Gorely stage shows the current Gorely cone, with steam emanating from the top. The image behind the ignimbrite series shows the sampling location in Opasny Ravine (Supplementary Data Fig. A2).

unit, and these fragments were sonicated in water for a minimum of 5 min and dried prior to being ground with a ceramic mortar and pestle. The standard used for the $^{87}Sr/^{86}Sr$ analyses was NBS987 and returned ratios of 0·710271 ± 11 and 0·710294 ± 11. The standard used for $^{143}Nd/^{144}Nd$ was JNdi-1, with ratios of 0·512098 ± 13 and 0·512097 ± 9. None of the ratios were normalized.

$^{40}Ar/^{39}Ar$ dating was undertaken on five ignimbrite units at the University of Wisconsin–Madison Rare Gas Geochronology Laboratory. Groundmass or matrix glass separates weighing ~200 mg were incrementally heated in a resistance furnace following the procedures of Jicha et al. (2012). Argon isotope analyses were made using a MAP 215-50 mass spectrometer with a single Balzers SEM-217 electron multiplier; the isotopic data were reduced using ArArCalc software version 2.5 (http://earthref.org/ArArCALC/). Atmospheric argon was measured 6–10 times prior to and following each incremental heating experiment. Measured $^{40}Ar/^{36}Ar$ ratios of atmospheric argon were normalized to $^{40}Ar/^{36}Ar = 295\cdot5$ (Steiger & Jäger, 1977). The age uncertainties reported in Supplementary Data Table A1 reflect analytical contributions only at the 2σ level and are calculated relative to the 28·201 Ma Fish Canyon sanidine standard (Kuiper et al., 2008); the decay constants used are those of Min et al. (2000).

Pyroxene and plagioclase major element compositions in selected ignimbrite units were determined using a Cameca SX100 electron microprobe at the University of Oregon MicroAnalytical Facility with a beam current of 30 nA, a beam energy of 15 keV, and a beam diameter of 10 μm. The counting time was 10 s for Ti and Cr, 20 s for K and Mn, 25 s for P, 30 s for Fe and Ca, 35 s for Si, and 40 s for Na, Al, and Mg.

RESULTS

Volcanic stratigraphy and dating of the major Gorely ignimbrites

We have expanded the pre-Holocene volcanic history of the Gorely eruptive center by identifying, characterizing, and dating the earliest exposed ignimbrite units found in the vicinity. As the age associations are complex, and based on various dating methods, this information is summarized in Fig. 4 and Table 1. In addition to the 361 ka date of Bindeman et al. (2010), we have determined $^{40}Ar/^{39}Ar$ ages for several more ignimbrite units in the area. Three samples produced statistically acceptable plateaux (three or more consecutive steps that contain >60% of the ^{39}Ar released) and have isochrons with trapped $^{40}Ar/^{36}Ar$ ratios that are indistinguishable from the atmospheric $^{40}Ar/^{36}Ar$ ratio of 295·5 (Table 1; Supplementary Data Table A1). For this reason, coupled with the observation that each $^{40}Ar/^{39}Ar$ age is consistent with its

Table 1: Method of age determination for Gorely samples

Sample no.	Latitude	Longitude	Rock type	Age determination	Age (ka)	2σ
11G-21	N52°32'16"	E157°58'31"	bomb	associated with 18th century fissure eruption	0·261	
11G-12	N52°31'25"	E157°59'07"	tephra	stratigraphic constraints	0·8	
11G-23	N52°33'13"	E158°02'23"	lava	associated with recent cone-building eruptions	1·5	
07L-54	N52°28'19"	E158°05'43"	lava	associated with recent eruption	2	
11G-4	N52°35'37"	E158°00'45"	lava	associated with recent eruption	2	
11G-24	N52°33'29"	E158°03'21"	lava	associated with recent cone-building eruptions	2	
11G-20	N52°35'10"	E158°03'04"	tephra	stratigraphic constraints	4	
11G-19	N52°35'10"	E158°03'04"	tephra	stratigraphic constraints	5	
11G-7	N52°31'25"	E157°59'07"	tephra	stratigraphic constraints	7	
11G-13	N52°35'06"	E158°03'34"	lava	stratigraphic constraints	7	
11G-14	N52°35'06"	E158°03'34"	lava	stratigraphic constraints	7	
11G-17	N52°34'35"	E158°05'16"	lava	stratigraphic constraints	7	
11G-18	N52°35'10"	E158°03'04"	tephra	stratigraphic constraints	7	
11G-8	N52°31'25"	E157°59'07"	tephra	stratigraphic constraints	8	
11G-9	N52°31'25"	E157°59'07"	tephra	stratigraphic constraints	8	
11G-10	N52°31'25"	E157°59'07"	tephra	stratigraphic constraints	8	
11G-5	N52°31'25"	E157°59'07"	lava	associated with early post-caldera monogenetic cone	20	
07L-53	N52°34'23"	E157°57'52"	ignimbrite	thin section petrography, $\delta^{18}O$	young ignimbrite series (38 ka)	
11G-3	N52°32'53"	E158°12'04"	pumice	$\delta^{18}O$, sample freshness, lack of burial	young ignimbrite series (38 ka)	
77L-144	N52°28'19"	E158°05'43"	ignimbrite	$^{40}Ar/^{39}Ar$*	young ignimbrite series (38 ka)	
109L-2010	N52°28'17"	E158°05'43"	ignimbrite	$^{40}Ar/^{39}Ar$	227	19
125L-2000	N52°30'01"	E158°07'57"	ignimbrite	thin section petrography, $\delta^{18}O$	227	
11G-1	N52°32'19"	E158°12'08"	ignimbrite	thin section petrography, $^{87}Sr/^{86}Sr$	300	
11G-2	N52°32'19"	E158°12'08"	ignimbrite	thin section petrography, $^{87}Sr/^{86}Sr$	300	
108L-2010	N52°28'17"	E158°05'47"	ignimbrite	$^{40}Ar/^{39}Ar$	324	10
107L-2010	N52°28'16"	E158°05'48"	ignimbrite	$^{40}Ar/^{39}Ar$	332	6
2005L-19	N52°37'31"	E158°05'49"	ignimbrite	$^{40}Ar/^{39}Ar$†	361	8
11G-6	N52°31'25"	E157°59'07"	lava	pra-Gorely lava‡	700	
11G-15	N52°35'14"	E158°05'03"	lava	pra-Gorely lava‡	700	
11G-16	N52°34'59"	E158°05'17"	lava	pra-Gorely lava‡	700	

*The $^{40}Ar/^{39}Ar$ age is <100 ka.
†Bindeman *et al.* (2010).
‡Pra-Gorely lavas are covered by 362 ka ignimbrites, and are intruded by 500 and 600 ka Karymshina dikes. They are also known to be younger than 800 ka Zhirovskoy deposits.

stratigraphic position, we consider the plateau ages to give the best estimate of the time elapsed since eruption. $^{40}Ar/^{39}Ar$ dates on welded tuffs from Opasny Canyon (Supplementary Data: Fig. A2) provide ages of 320–330 ka for the lower two units, ~230 ka for the middle units, and an age of <100 ka for the upper, youngest ignimbrite in this section (77L-l44). Two more ignimbrites, which stratigraphically overlie the '<100 ka' ignimbrite, have been described near Opasny Canyon, but were not dated in this study. The lower of these units is welded whereas the upper is a non-welded layer of pumice, which is probably related to the pumice exposed in other directions from the Gorely caldera. The upper three ignimbrite units are not dated and probably fit stratigraphically into the <l00–38 ka interval.

Older ignimbrites are partly eroded, covered with younger products, and cannot be mapped individually. Therefore, we have to make assumptions about the age of some samples, which have unclear stratigraphic context (Fig. 4; Table 1). Based on similar thin section petrography (higher plagioclase abundance and similar amount of groundmass) and $\delta^{18}O$ to unit 77L-l44, unit 07L-53 was assigned a tentative age of 38 ka in accordance with a correlated pumice deposit (Braitseva *et al.*, l995). Units llG-l

and 11G-2 (lower and upper portion of the same ignimbrite) in the Falshivaya River failed to produce an $^{40}Ar/^{39}Ar$ age. Despite this, we have assigned this ignimbrite a tentative age of ~300 ka, because of its close association with 2005L-19, based on $^{87}Sr/^{86}Sr$ and thin section petrography. Pumice samples 11G-3a/b were found on the surface, and are grouped with the 38 ka (younger ignimbrite) samples, given the lack of weathering and apparent freshness of the sample, lack of burial by subsequent deposits, and similar $\delta^{18}O$ value to unit 77L-144.

U–Pb zircon geochronology

We attempted to extract zircons from the studied ignimbrites by HF dissolution of bulk rocks, but all were zircon-undersaturated; only one xenocryst was extracted from a pumice sample (11G-3a) that yielded Eocene U–Pb ages of $54·7 \pm 1·1$ Ma (1SE) (core) and $37·5 \pm 0·7$ Ma (1SE) (rim), suggesting the presence of material underlying the Gorely eruptive center of this age. Rocks of Cretaceous–Eocene age are common in eastern Kamchatka, including the crust of the 45–50 Ma Achaivayam–Valaginsky Arc. The Th/U ratios of this zircon (0·02 for the rim and 0·11 for the core) suggest metamorphic derivation (Rubatto, 2002) and a collision-type origin, which we correlate with the Achaivayam–Valaginsky Arc. Furthermore, the Ganal Massif (Fig. 1), which is a portion of the metamorphic basement of the Achaivayam–Valaginsky Arc, contains zircons with ages ranging between 15 and 40 Ma as well as between 55 and 85 Ma, showing two separate metamorphic events. The older age relates to the accretion of the Ganal Massif onto Kamchatka, whereas the younger age reflects the accretion of the eastern Kamchatka Peninsula (Bindeman et al., 2002). These age ranges overlap with both the rim and core of the zircon xenocryst from the Gorely eruptive center.

Zircons from the Akhomten Massif were also dated by the U–Pb method, yielding an age of $11·2 \pm 0·08$ Ma (1SE). This age slightly predates the established timing of the accretion of the Kronotski arc (10–7 Ma). Furthermore, zircons from three Qtz–Bi-bearing ignimbrite units that probably underlie the Gorely eruptive center were dated by the U–Pb method, and all returned ages near 4 Ma (Supplementary Data: Table A1). These ages are older than those currently known for units erupted from the nearby Zhirovskoy (0·67–0·84 Ma; Sheimovich & Karpenko, 1996) and Karymshina (~1·5–2·0 Ma; Bindeman et al., 2010) eruptive centers, and therefore suggest longer-lived silicic volcanism and magmatism in this region. Compositionally, they are similar to younger Karymshina ignimbrites.

Major element geochemistry of the eruptive products

Newly obtained and compiled analyses of the Gorely eruptive products range from ~52 to 69 wt % SiO_2 (Table 2),

but include only sparse amounts of andesite. This shows a clear bimodal distribution or 'Daly Gap' present in the Gorely eruptive products (Figs 5 and 6), which will be addressed later in the discussion. Sampling bias is assumed to be minimal owing to our range of sample collection, which was not focused on a particular type of sample (e.g. rhyolite vs basalt), and owing to our compilation of previously published data from the GEOROC database.

The variation of SiO_2 content (wt %) versus newly determined $^{40}Ar/^{39}Ar$ ages, and previously determined ^{14}C Holocene ages (calibrated with the help of Calib 6.0; Selyangin & Ponomareva, 1999) is illustrated in Fig. 5a. The established stratigraphy demonstrates that following a nearly 700 kyr period of dominantly dacitic ignimbrite eruptions at the Gorely eruptive center, there was a shift in eruptive compositions at 38 ka to predominantly basalt and basaltic andesite (Fig. 5a). This change is illustrated in nearly all the material erupted prior to 38 ka (including the pra-Gorely cone-building stage and the ignimbrite series) being dacitic, whereas the material that forms the modern (younger than 38 ka) Gorely cone is nearly all basalt to basaltic andesite in composition. Although this is the surficial expression of the Gorely magmatism, an older, small volume of basalt from previous Gorely eruptions could be buried.

In addition to analyzing Gorely rocks, we also studied the eruptive products of nearby silicic centers to confirm that our samples are sourced from Gorely volcano, which is possible because of the strong across-arc geochemical zonation in Kamchatka (Ponomareva et al., 2007). It is of particular importance to note the differences in chemical composition between the Gorely ignimbrites, which are all similar to one another (e.g. Fig. 7c), and the material erupted from Mutnovsky. This is important because the ignimbrites collected from Opasny Canyon, which is located near Mutnovsky volcano, were in fact erupted from Gorely (Fig. 2). Gorely magmas are predominantly calc-alkaline in an AFM diagram and follow the boundary between tholeiitic and calc-alkaline series. Figure 7 demonstrates across-arc geochemical changes from the volcanic front (Mutnovsky) to Gorely, and then to Opala in the rear arc of the Kamchatkan subduction zone (Fig. 1). This may be due to the increased depth of the subducting slab and decreasing degree of mantle melting (Walker et al., 1995; Ishikawa & Tera, 1997; Taylor & Nesbitt, 1998; Churikova et al., 2001; Hochstaedter et al., 2001). Mutnovsky magmas in the volcanic front are more depleted in K_2O relative to Gorely (Fig. 7c), whereas Opala magmas from the back-arc have similar K_2O contents to Gorely; Karymshina magmas have a wider range in K_2O. Gorely dacites have slightly elevated Na_2O concentrations relative to Mutnovsky, Opala, and Karymshina products (Fig. 7b), whereas more mafic materials from these eruptive centers generally have the same Na_2O

Table 2: Major (wt %; normalized to 100%) and trace element (ppm) XRF compositions of Gorely eruptive products and a granite from the Akhomten Massif

Sample no.:	11G-21	11G-12	11G-23	07L-54	11G-24	11G-4	11G-20	11G-19
Age (Ma):	MG	MG	MG	MG	MG	MG	MG	MG
SiO_2	57·1	53·6	54·7	64·6	56·7	56·2	55·0	52·1
TiO_2	1·13	0·78	1·24	1·02	1·12	1·35	1·16	1·11
Al_2O_3	16·7	17·0	16·8	15·4	16·4	15·4	17·1	18·7
FeO^T	8·10	8·51	9·37	5·50	8·29	9·05	8·26	8·96
MnO	0·16	0·17	0·16	0·13	0·16	0·17	0·16	0·16
MgO	4·00	6·70	4·67	1·59	4·55	4·89	4·79	5·59
CaO	7·05	9·59	7·83	3·95	6·92	6·78	7·95	8·81
Na_2O	3·55	2·64	3·24	4·26	3·54	3·43	3·35	3·16
K_2O	1·88	0·80	1·60	3·19	1·96	2·23	1·73	1·03
P_2O_5	0·38	0·13	0·41	0·36	0·39	0·49	0·41	0·32
Total*	98·90	99·90	98·00	98·90	99·00	99·30	97·60	96·90
Ni	31	34	38	4	42	56	51	56
Cr	53	93	75	5	96	125	117	119
Sc	26	35	28	17	25	27	27	28
V	206	235	241	99	198	231	209	233
Ba	514	240	492	794	539	574	468	328
Rb	36	15	30	64	36	44	32	17
Sr	411	379	432	307	425	366	441	479
Zr	189	75	181	290	197	236	182	120
Y	32	20	34	40	33	39	32	25
Nb	6·3	2·0	6·2	7·9	6·2	7·9	6·2	3·9
Ga	17	17	17	18	18	16	18	18
Cu	69	90	72	13	61	112	98	90
Zn	82	85	90	72	82	94	78	74
Pb	9	6	5	13	9	11	8	5
La	15	5	18	24	17	21	11	13
Ce	41	13	42	52	38	52	33	33
Th	3	1	3	5	3	3	2	2
Nd	25	13	26	31	24	30	25	19
U	2	1	0	3	0	2	2	0

Sample no.:	11G-7	11G-13	11G-14	11G-17	11G-18	11G-10	11G-8	11G-9
Age (Ma):	MG	MG	MG	MG	MG	MG	MG	MG
SiO_2	54·2	56·5	65·8	56·2	55·1	62·8	52·8	54·0
TiO_2	1·08	1·03	1·02	1·11	1·05	1·15	1·07	1·03
Al_2O_3	18·6	17·6	15·0	16·6	18·1	15·8	18·5	19·2
FeO^T	8·13	7·63	5·20	8·33	8·06	6·22	8·92	8·61
MnO	0·15	0·15	0·13	0·16	0·16	0·15	0·16	0·17
MgO	4·30	4·10	1·42	4·64	4·70	1·94	5·43	3·59
CaO	8·50	7·32	3·41	7·10	7·47	4·55	8·56	8·63
Na_2O	3·41	3·60	4·27	3·53	3·42	4·35	3·15	3·29
K_2O	1·32	1·79	3·43	1·87	1·56	2·66	1·08	1·23
P_2O_5	0·37	0·35	0·36	0·38	0·36	0·33	0·32	0·30

Table 2: Continued

Sample no.:	11G-7	11G-13	11G-14	11G-17	11G-18	11G-10	11G-8	11G-9
Age (Ma):	MG	MG	MG	MG	MG	MG	MG	MG
Total*	97·20	99·00	98·10	98·90	97·40	98·00	96·50	96·30
Ni	28	37	4	44	50	4	54	19
Cr	53	80	6	94	99	4	96	47
Sc	26	22	16	25	24	20	26	27
V	212	172	86	192	183	125	218	218
Ba	462	505	834	530	463	730	393	427
Rb	22	32	69	35	27	49	19	23
Sr	550	469	264	444	468	358	511	491
Zr	139	185	311	191	173	262	122	132
Y	25	31	42	33	31	39	24	25
Nb	4·5	5·9	8·4	5·9	5·9	7·8	3·8	5·0
Ga	19	19	17	17	18	17	18	17
Cu	69	36	13	59	84	28	82	68
Zn	76	74	72	81	84	86	82	71
Pb	6	7	15	8	8	12	5	6
La	17	16	22	19	17	21	12	11
Ce	35	39	59	39	35	48	29	26
Th	2	2	6	4	2	4	2	2
Nd	23	25	31	25	23	28	20	17
U	1	0	3	3	1	1	0	0

Sample no.:	11G-5	07L-53	11G-3	77L-144	11G-15	11G-16	11G-6	125L-2000
Age (Ma):	MG	I	I	I	PG	PG	PG	I
SiO_2	52·1	64·7	66·9	63·7	68·2	61·2	65·1	65·8
TiO_2	1·32	1·06	0·80	1·00	0·91	1·44	1·00	1·11
Al_2O_3	17·1	16·4	15·7	16·6	15·1	15·2	16·2	15·5
FeO^T	9·94	4·61	3·98	5·22	3·73	7·70	4·49	4·85
MnO	0·18	0·17	0·11	0·16	0·14	0·19	0·15	0·17
MgO	4·91	1·49	1·25	1·68	0·89	2·01	1·41	1·34
CaO	9·77	3·51	3·08	4·13	2·30	4·58	3·53	3·04
Na_2O	3·31	5·30	4·78	4·96	5·22	4·55	5·19	5·05
K_2O	1·01	2·53	3·20	2·29	3·27	2·52	2·66	2·90
P_2O_5	0·41	0·23	0·23	0·31	0·21	0·59	0·32	0·26
Total*	99·2	98·1	94·8	99·3	98·1	98·5	98·8	98·47
Ni	19	3	5	6	3	4	2	5
Cr	42	7	5	4	3	3	3	5
Sc	36	17	14	18	15	24	16	18
V	320	49	75	96	36	129	51	61
Ba	410	752	767	671	895	727	732	836
Rb	14	43	52	37	59	45	46	51
Sr	604	384	249	362	241	348	342	297
Zr	113	251	295	246	326	258	263	295
Y	27	43	39	41	51	48	43	48
Nb	6	9	10	8	10	9	8	10
Ga	19	18	16	19	18	19	19	18
Cu	104	2	15	18	3	14	3	6

(continued)

(continued)

Table 2: Continued

Sample no.:	11G-5	07L-53	11G-3	77L-144	11G-15	11G-16	11G-6	125L-2000
Age (Ma):	MG	I	I	I	PG	PG	PG	I
Zn	91	95	63	84	80	106	78	93
Pb	5	11	14	10	15	11	10	13
La	14	23	21	19	28	27	26	27
Ce	29	55	52	47	61	57	52	60
Th	1	3	4	4	4	3	3	4
Nd	22	32	26	27	37	34	32	35
U	0	1	1	2	2	2	1	1

Sample no.:	109L-2010	11G-1	11G-2	108L-2010	107L-2010	2005L-19	89L-9†
Age (Ma):	0·227	I	I	0·324	0·332	0·361‡	11·2§
SiO_2	63·3	68·1	67·1	62·1	66·2	65·6	74·3
TiO_2	1·10	0·93	0·99	1·21	0·91	0·94	0·30
Al_2O_3	16·6	15·3	15·7	16·6	16·2	16·2	13·3
FeO^T	5·49	3·86	4·11	5·81	4·14	4·21	2·09
MnO	0·18	0·13	0·12	0·19	0·15	0·16	0·60
MgO	1·67	0·78	0·80	1·81	0·88	1·26	0·04
CaO	3·97	2·21	2·39	4·47	2·93	3·24	1·72
Na_2O	4·87	5·20	4·94	4·99	5·35	5·36	4·48
K_2O	2·41	3·27	3·57	2·23	2·93	2·69	3·15
P_2O_5	0·40	0·21	0·24	0·52	0·26	0·27	0·06
Total*	97·4	98·1	98·1	100	98·9	99·5	99·99
Ni	4	6	6	3	4	0	1
Cr	3	5	4	4	4	2	9
Sc	19	16	17	21	17	17	7
V	70	40	47	89	46	45	41
Ba	597	902	874	679	795	783	1061
Rb	38	56	64	34	57	47	109
Sr	348	242	265	432	323	348	156
Zr	223	326	313	222	275	270	172
Y	45	55	48	43	47	48	22
Nb	8	10	11	8	9	8	4
Ga	19	17	18	19	19	18	13
Cu	8	12	13	10	6	4	12
Zn	97	82	83	105	87	81	33
Pb	9	16	14	12	14	10	13
La	21	28	26	21	24	23	15
Ce	48	67	66	54	58	55	28
Th	3	4	5	4	4	3	9
Nd	30	39	36	34	37	33	7
U	0	1	2	0	1	1	3

MG, modern Gorely; PG, pra-Gorely; I, ignimbrite; ages with a specific value are from $^{40}Ar/^{39}Ar$ dating.
*Non-normalized total included.
†89L-9 is a fine-grained granodiorite of the Akhomten Massif.
‡Data from Bindeman *et al*. (2010).
§U–Pb age.

concentration. In contrast, Gorely magmas have CaO concentrations that are lower than those of Mutnovsky, Opala, and Karymshina (Fig. 7a). Nearly all the Gorely magmas have a higher P_2O_5 concentration (peaking at $\sim$60 wt % SiO_2) than material erupted from Opala, Mutnovsky, and Karymshina volcanoes (Fig. 7d). Additional major element variation diagrams are included in Supplementary Data Fig. A3.

Petrography of the erupted products

The petrography of 14 representative Gorely units (eight ignimbrites and six lavas) is summarized in Table 3.

Ignimbrites

Phenocrysts in all units include plagioclase + orthopyroxene + clinopyroxene + magnetite ± apatite. Plagioclase abundance in the ignimbrite units ranges from 5 to 11%, whereas pyroxene ranges from 3 to 10% (both are $\sim$0·5–6 mm in length). Groundmass, glass and vesicle abundance is in the range of 58–81%, 5–30% and 1–20% respectively. Ignimbrite units typically have a groundmass that is variable on a thin section scale, with both devitrified and glassy varieties, colors ranging from gray to black, and some clasts containing abundant plagioclase microlites (Supplementary Data: Fig. A4). Many ignimbrites contain sieve-textured plagioclase and pyroxene grains, indicating resorption, with unit 125L-2010 having the largest proportion of euhedral grains. The youngest and oldest ignimbrite units do not differ markedly in terms of their petrography. Six of the eight ignimbrites contain glomeroporphyritic aggregates of plagioclase, clinopyroxene, and orthopyroxene. The minerals in these clusters are not elongated and therefore do not indicate crystal compaction prior to eruption. The proportion of glomeroporphyritic aggregates among total crystals ranges from 1 to 25% (Supplementary Data: Fig. A5). The degree of resorption of crystals in glomerocrysts is variable, with the most resorption in unit 07L-53, whereas units 125L-2000 and 11G-2 contain many large crystal clusters without much resorption.

All ignimbrites contain small mafic enclaves (Supplementary Data: Fig. A6), ranging in size from $\sim$1 mm up to $\sim$1 cm in diameter, with most being around 2 mm. The enclaves are oval in shape (Supplementary Data: Fig. A6), with a groundmass of plagioclase microlites. The plagioclase and pyroxene phenocrysts within the enclaves are predominantly euhedral, although in unit 77L-144 they are mostly resorbed.

Lavas

Lava units contain 11–30% of the same phenocryst assemblage of plagioclase + clinopyroxene + orthopyroxene + magnetite ± apatite, of which 1–7% is contained in glomeroporphyritic aggregates. Unlike the ignimbrite units, some of the lava units also contain olivine
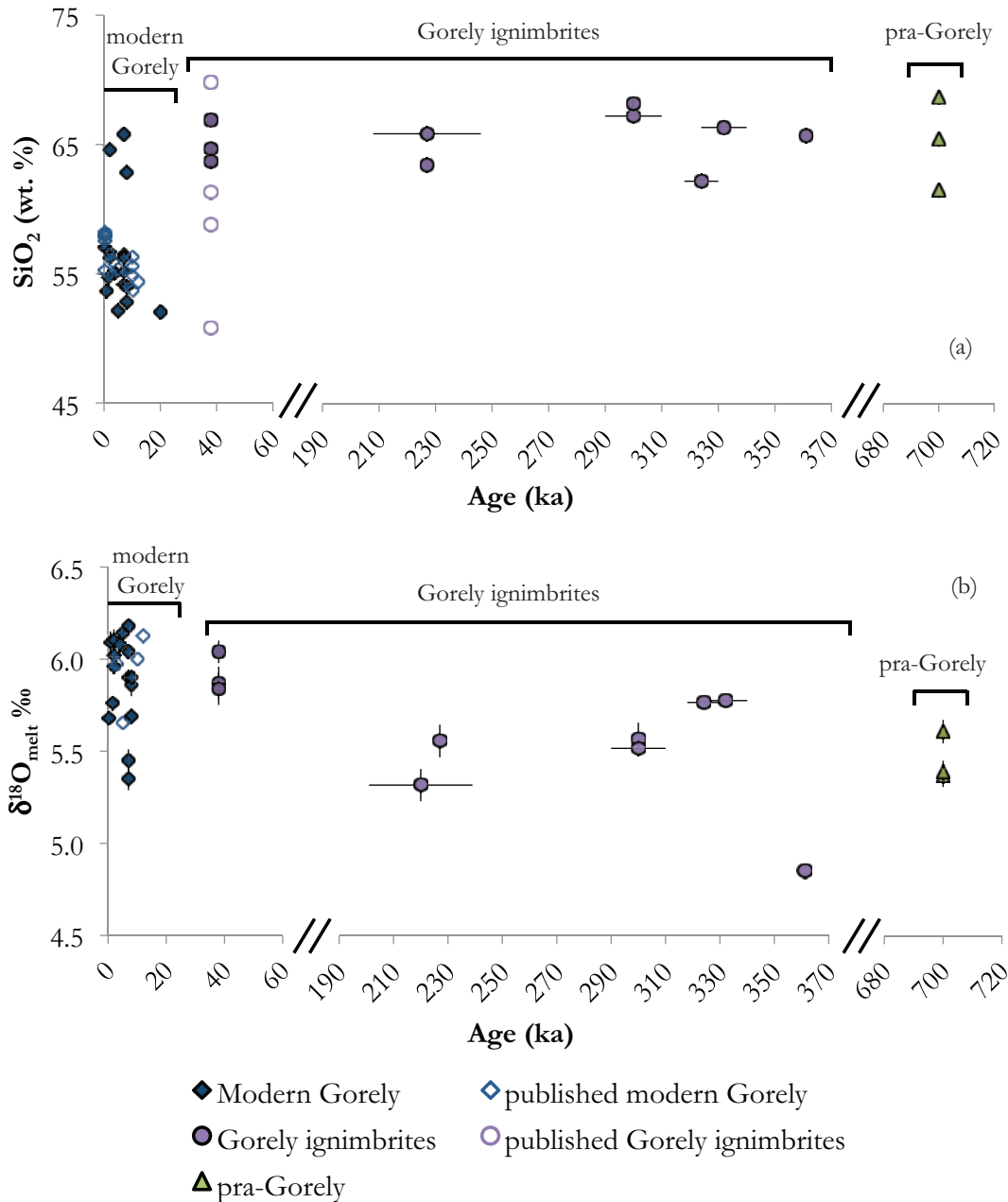
Fig. 5. Temporal evolution trends for Gorely magmas. (a) Age vs SiO_2 wt % ($\pm 2\sigma$). (b) Age vs $\delta^{18}O_{melt}$ ($\pm 1SE$). Four dated ignimbrites are plotted: 109L-2010 (227 ka), 108L-2010 (324 ka), 107L-2010 (332 ka) and 2005L-19 (361 ka). All other ages are based on stratigraphic order or associations with other units (Table 1). Published Gorely ignimbrite data (SiO_2) are from Duggen *et al.* (2007), and the age for ignimbrite 2005L-19 (361 ka) is from Bindeman *et al.* (2010). The break in time between pra-Gorely and the early ignimbrite series, and between the old and young ignimbrites, should be noted.

(modern Gorely: 11G-13, 11G-21, 11G-24) and amphibole (pra-Gorely: 11G-6) phenocrysts. The abundance of plagioclase and pyroxene ranges from 2 to 17% and from 5 to 11% respectively, with size ranging from ~0·5 to 3 mm length. In comparison with the ignimbrites, the lavas have slightly larger amounts of plagioclase, although the range in pyroxene abundance is similar between the two. Groundmass and vesicle abundances range from 70 to

89% and from 0 to 60% respectively, with no units containing pristine glass (Table 3). The groundmass varies from abundant plagioclase microlites to devitrified glass. Some units show evidence of resorption in their phenocrysts, with 11G-21, 11G-24, and 11G-13 (all modern Gorely units) showing the most resorption.

Only one lava (11G-14; modern Gorely) contains mafic enclaves (~2 mm wide and 3–4 mm long) in a groundmass
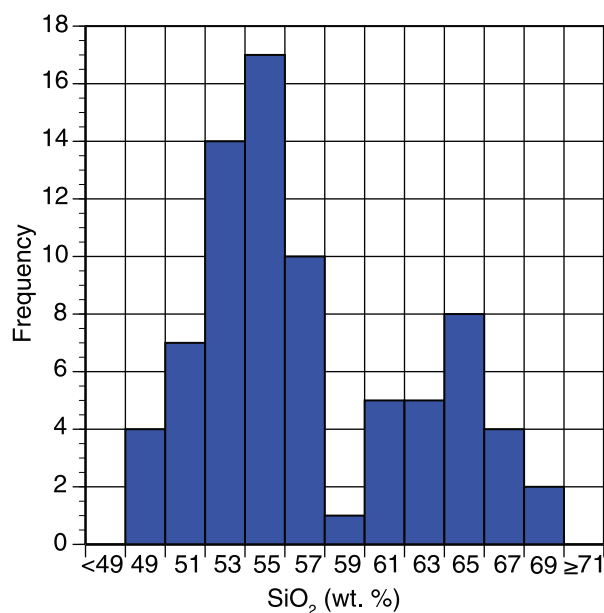
Fig. 6. Histogram of SiO_2 (wt %) variation for all Gorely units, including data from the literature (GEOROC database; http://georoc.mpch-mainz.gwdg.de/georoc/). Each bin is labeled with the lower SiO_2 wt % value, and spans 2 wt % SiO_2. The histogram shows the bimodality of the rock compositions from Gorely volcano, displaying a clear Daly Gap. Data are from this work and from Popolitov & Volynets (1981), Kepezhinskas et al. (1997), Pineau et al. (1999), Ishikawa et al. (2001), Duggen et al. (2007) and Chashchin et al. (2011).

of plagioclase microlites and rare plagioclase and pyroxene crystals ($\sim$0·5–2 mm).

Trace element variations

Trace elements show separate trends between the andesites–dacites and the basalts–basaltic andesites in terms of K_2O, Rb, Ba, and Sr concentrations at constant SiO_2 (Figs 8 and 9). Although the relative incompatibility and subsequent concentration of K_2O, Rb, and Ba will vary based on the crystallizing assemblage, offsets of this magnitude cannot be produced from closed-system fractional crystallization. The entire ignimbrite series falls on the same trends, signifying a common parental melt or source rock under Gorely for all the ignimbrites in this study. Figure 9 shows the trace element trends with respect to Zr. Zirconium should be a highly incompatible element in the zircon-undersaturated Gorely magmas. Although the trends are less clear in Fig. 9, the offset is still obvious in the Rb and Ba plots. Overall, these elemental trends clearly illustrate that fractional crystallization of basalt at one or multiple depths (see below) is incapable of explaining the extended magmatic series of Gorely to produce the dacites.

Pyroxene and plagioclase chemistry

Gorely ignimbrites contain both clinopyroxene and orthopyroxene, both of which are largely unzoned (Table 4; Supplementary Data Fig. A7). Pyroxene chemistry does not appear to vary consistently between grains and those that are contained within aggregates. The presence of xenocrysts among the orthopyroxenes from 11G-2 is suggested by the larger variation, although there is no significant variability between the cores and rims of these pyroxene grains. Plagioclase in the Gorely ignimbrites ranges from An_{35} to An_{48}. One plagioclase aggregate was analyzed, and is towards the higher end of An content for Gorely ignimbrites (Table 5).

Isotopic variations

$\delta^{18}O$ values of coexisting plagioclase and pyroxene grains as well as groundmass samples were determined for all units, and these were used to calculate the melt $\delta^{18}O$ values (Table 6). $\delta^{18}O_{plag}$ values range from 4·53 to 6·18‰, and the $\delta^{18}O_{melt}$ values from 4·85 to 6·41‰ (Table 6). This is a fairly wide range for any single arc volcano, with values ranging from normal $\delta^{18}O$ (between $\sim$5·5 and 6·5‰), which could be produced by fractional crystallization of a mantle-derived basalt, to distinctly low $\delta^{18}O$ ($<$5·7‰), which requires assimilation of moderate amounts of low-$\delta^{18}O$ hydrothermally altered material. The low $\delta^{18}O$ values characterize both silicic and mafic units. These units are spaced somewhat randomly throughout the evolution of the Gorely eruptive center, with two being from the 'pra-Gorely' stage $\sim$0·7 Ma (11G-6 and 11G-16), two erupting during the early ignimbrite eruptions at 0·361 and 0·220 Ma (2005 L-19 and 125L-2010 respectively), and the last two being from the modern Gorely stage (11G-17 and 11G-18).

These $\delta^{18}O$ variations through time are shown in Fig. 5b, where there is a small range in $\delta^{18}O_{melt}$ during the pra-Gorely stage of cone-building (the cone present prior to the earliest known caldera-forming eruptions). The range in $\delta^{18}O_{melt}$ (4·85–5·78‰) is then at its largest in the early ignimbrite series of eruptions, when it also contains the lowest $\delta^{18}O_{melt}$ value (4·85‰). The range then decreases significantly (with only normal $\delta^{18}O_{melt}$ values) during the younger ignimbrite series at 38 ka (Fig. 5b). The modern Gorely series of eruptions (younger than 38 ka) shows an increase in $\delta^{18}O_{melt}$ range (5·38–6·22‰).

The $^{87}Sr/^{86}Sr$ and $^{143}Nd/^{144}Nd$ compositions of major ignimbrites from the Gorely eruptive center are in the range of 0·70328–0·70351 and 0·51303–0·51309 respectively (Table 6). These ranges are higher ($^{87}Sr/^{86}Sr$) and lower ($^{143}Nd/^{144}Nd$) than average Kamchatkan mantle values (0·70275 and 0·51310, respectively) as reported by Duggen et al. (2007) based on hypothetical isotopic endmember estimates. These instead trend towards a crustal endmember, and overlap with other silicic rocks from the area (notably Akhomten and Karymshina; see discussion below) (Fig. 1).
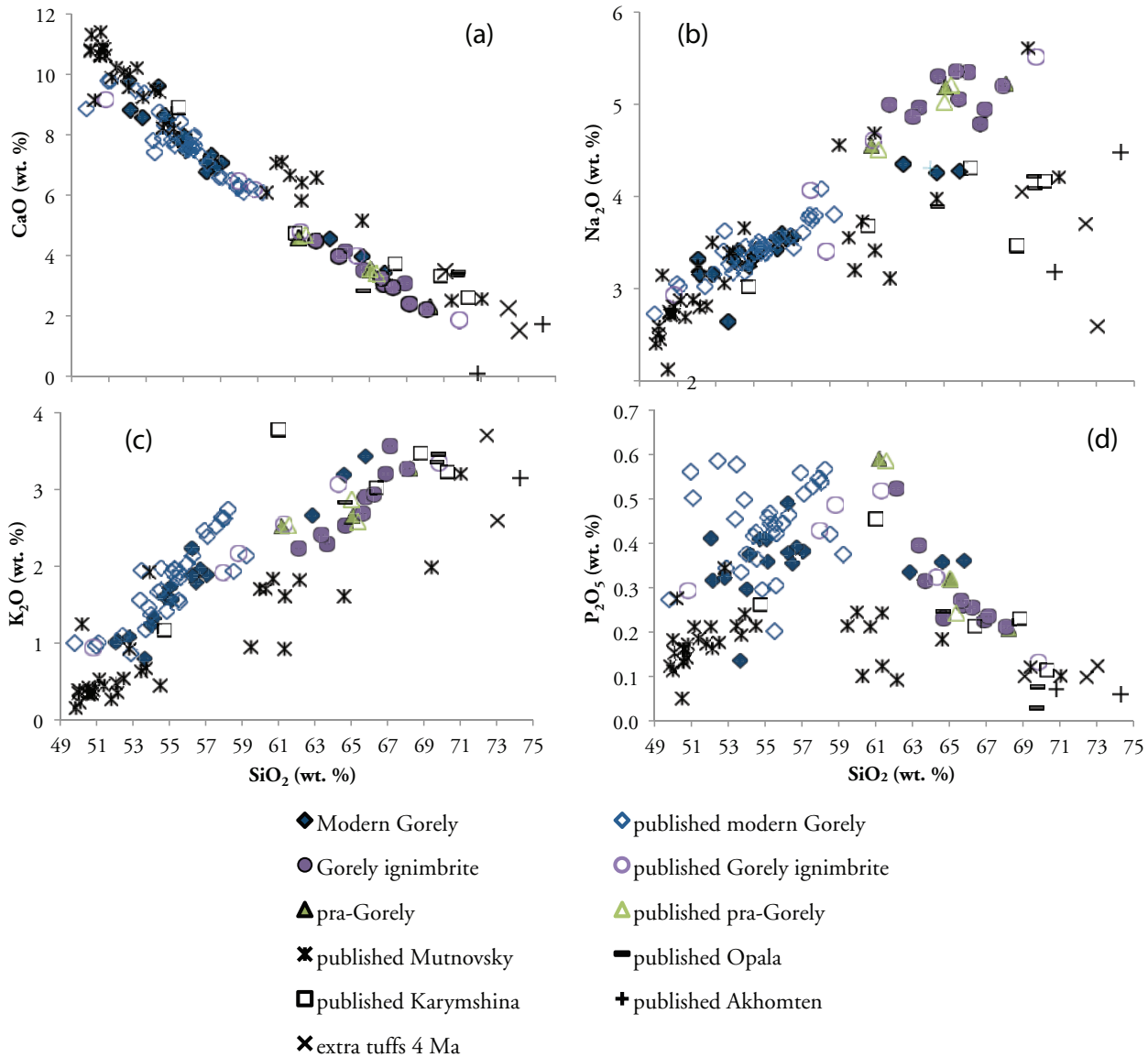
Fig. 7. Major element compositional variations within the Gorely eruptive rocks compared with nearby volcanic centers (Mutnovsky, Opala, Karymshina, and nearby 4 Ma tuffs—see Figs 1 and 2). Gorely data are from this study and those listed in the caption to Fig. 6. Karymshina data are from Shipley (2011); Mutnovsky data are from Poplitov & Volynets (1981), Hochstaedter *et al.* (1996), Kepezhinskas *et al.* (1997), Pineau *et al.* (1999), Bindeman *et al.* (2004) and Duggen *et al.* (2007); Opala data are from Bindeman *et al.* (2004).

Thermometry and barometry results

The $\delta^{18}O$ values of coexisting plagioclase and pyroxene were used to determine the magmatic temperature based on isotopic fractionation between $\delta^{18}O_{plag}$ and $\delta^{18}O_{pyx}$ using Chiba *et al.* (1989) A-factors (Fig. 10, Table 6). We used the known $\delta^{18}O$ of each mineral, and the measured anorthite content of the plagioclase, as A-factors change $\sim 0\cdot 1\%$ per 10% change in anorthite. Uncertainties for this method are based on the analytical error of the $\delta^{18}O$ analysis (2σ up to $0\cdot 15\permil$), the chosen anorthite content (discussed below), and the A-factor needed to determine the temperature of a given plagioclase–pyroxene

fractionation [standard error of $0\cdot 09$ from Chiba *et al.* (1989)]. The $\delta^{18}O$ analyses were conducted on multiple whole crystals, with weights ranging from 1 to 2 mg, and are therefore representative of the average for a batch of crystals. Pyroxenes do not exhibit significant compositional zoning, whereas plagioclase shows both normal and reverse zoning, with a variation of ~ 10 An units for all the ignimbrites analyzed.

Temperatures were determined for modern Gorely basalt to basaltic andesite using an An_{65} plagioclase composition, which is the average An composition observed by Tolstykh *et al.* (2012) for basalt to basaltic

Table 3: Thin section petrography of the Gorely eruptive products

Sample no.:	77L-144	11G-2	107L-2010	07L-53	11G-21	11G-14	11G-6
Rock type:	ignimbrite	ignimbrite	ignimbrite	ignimbrite	bomb	lava	lava
plagioclase (%)	9	7	5	11	5	6	2
opx (%)	5	5	2	3	3	4	3
cpx (%)	2	5	1	7	5	7	2
glass (%)	25	20	30	10	0	0	0
vesicles (%)	12	10	5	5	40	2	0
groundmass (%)	58	62	61	66	85	81	89
olivine (%)	0	0	0	0	2	0	0
amphibole (%)	0	0	0	0	0	0	1
magnetite (%)	1	1	1	3	0	2	3
mineral abundance (%)	17	18	9	24	15	19	11
crystals in clusters (%)	3	5	1	5	3	7	5
approximate grain size (mm)	1–2	0·5–2	0·5–2	1–2	0·5–2	0·5–2	1–2
mafic enclaves	yes	yes	yes	yes	no	yes	no
plagioclase zoning	N/R	R	N/R	N/R	N/R	N/R	N/R
sieve texture*	X		X		X		

Sample no.:	109L-2010	108L-2010	07L-54	11G-13	11G-24	2005L-19	125L-2000
Rock type:	ignimbrite	ignimbrite	lava	lava	lava	ignimbrite	ignimbrite
plagioclase (%)	5	4	7	17	7	6	5
opx (%)	2	2	3	5	3	3	4
cpx (%)	1	1	7	5	4	5	3
glass (%)	10	10	0	0	0	5	5
vesicles (%)	1	20	0	60	35	10	1
groundmass (%)	80	81	80	70	82	80	81
olivine (%)	0	0	0	3	4	0	0
amphibole (%)	0	0	0	0	0	0	0
magnetite (%)	2	2	3	0	0	1	2
mineral abundance (%)	10	9	20	30	18	15	14
crystals in clusters (%)	0	0	5	1	1	3	25
approximate grain size (mm)	0·5–1	0·5–2	0·5–2	0·5	0·5–2	0·5–2	0·5–4
mafic enclaves	significant amount	significant amount	no	no	no	yes	yes
plagioclase zoning	N/R	N/R	N/R	R	N/R	N/R	N/R
sieve texture*	trace	X		X	X	X	

Mineral abundances were determined by taking all the minerals of each type in the field of view (i.e. plagioclase, opx, cpx) and visually clustering them into a corner of the field of view and approximating the per cent of the field of view that the mineral covers. This was done at least 15 times for each thin section, and the percentage for each mineral was averaged for that unit. opx, orthopyroxene; cpx, clinopyroxene; N, normal zoning; R, reverse zoning.
*X signifies a greater amount of the texture and includes both plagioclase and pyroxene minerals.
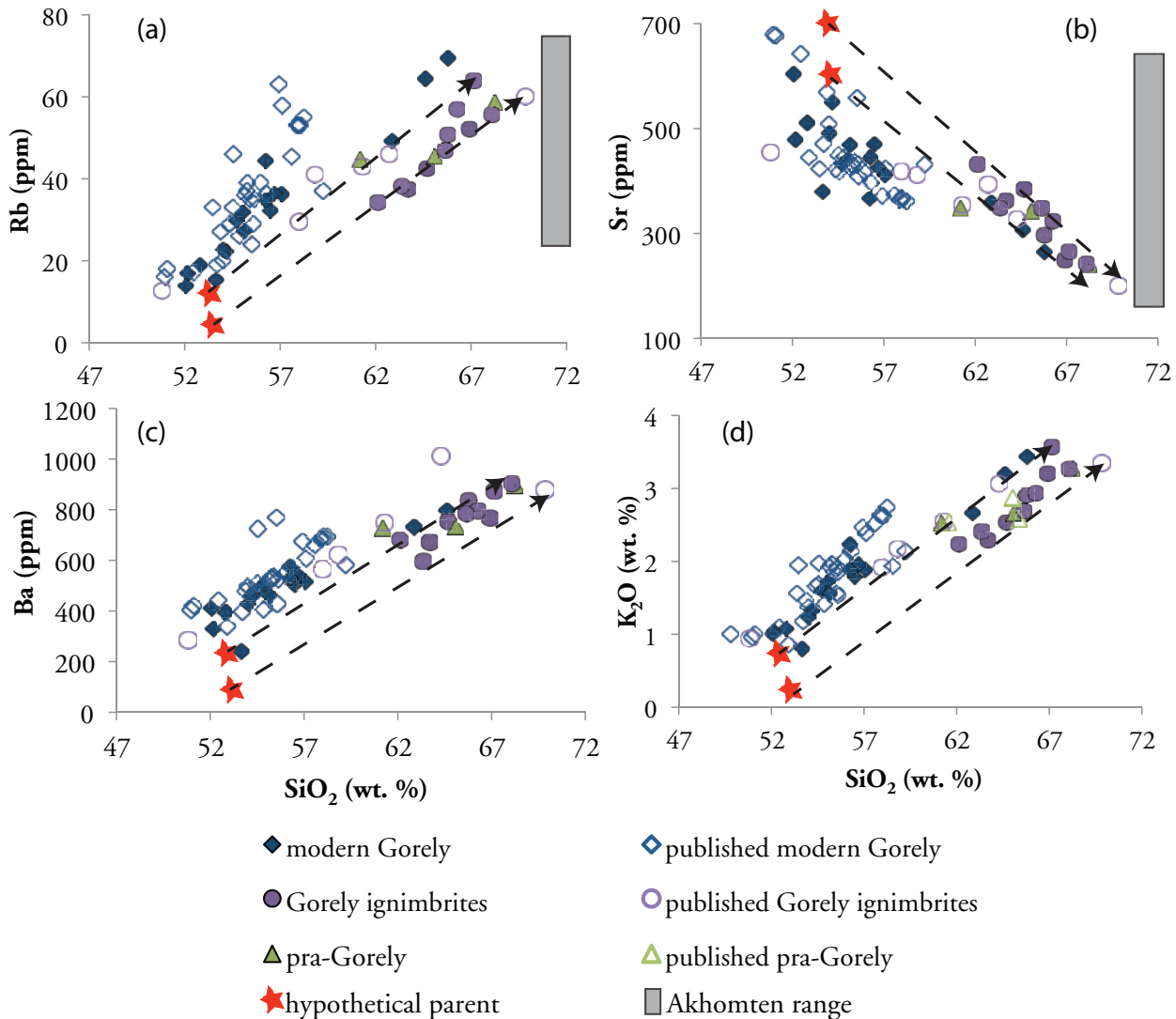
Fig. 8. Harker variation diagrams showing two separate trends for basic (49–59 wt % SiO_2) and silicic (62–69 wt % SiO_2) subgroups of rocks. If fractional crystallization were the only process occurring, K_2O, Rb, Ba, and Sr should all follow smooth and continuous trends, which is not the case. Dashed arrows indicate possible fractionation trends from two hypothetical parent magmas (indicated by red stars) that are different from the parent magma of the basalts–basaltic andesites. Error bars are smaller than the symbol size. Data for Gorely are from this study and sources listed in the Fig. 6 caption. Data for the Akhomten Massif are from this study and Vinogradov (1995).

andesites from the Gorely eruptive center. Temperatures for the dacites (pra-Gorely lavas and ignimbrites) were determined using An_{43}, based on the average An composition of plagioclase in the dacitic ignimbrites analyzed from this study, which is similar to that documented by Tolstykh *et al.* (2012). If the dacitic An content is decreased from An_{43} to An_{35} (the lowest An content determined here), this will cause an average increase in temperature of 44°C, and if An_{48} is used (the highest An content found in this study) the temperature will decrease by an average of 26°C. If the An content was increased by 10 to An_{75} or decreased by 10 to An_{55} for the basalt to basaltic andesite samples, the temperature would decrease by an

average of 59°C or increase by an average of 58°C, respectively.

Our $\delta^{18}O$ data demonstrate well that both plagioclase and pyroxene record a 1·7‰ range in $\delta^{18}O$ values at magmatic temperatures (Fig. 10), illustrating diverse $\delta^{18}O$ magma compositions. Using realistic An % and plagioclase–pyroxene A-factors, temperatures range from ~1230 to 780°C, and we observe no particular distinction in temperature between magmas of diverse composition or age. The ignimbrites plot in a magmatic range of temperatures from 1230 to 890°C, although the higher of these isotopic temperatures are unusually high for dacites (Fig. 10, Table 6).
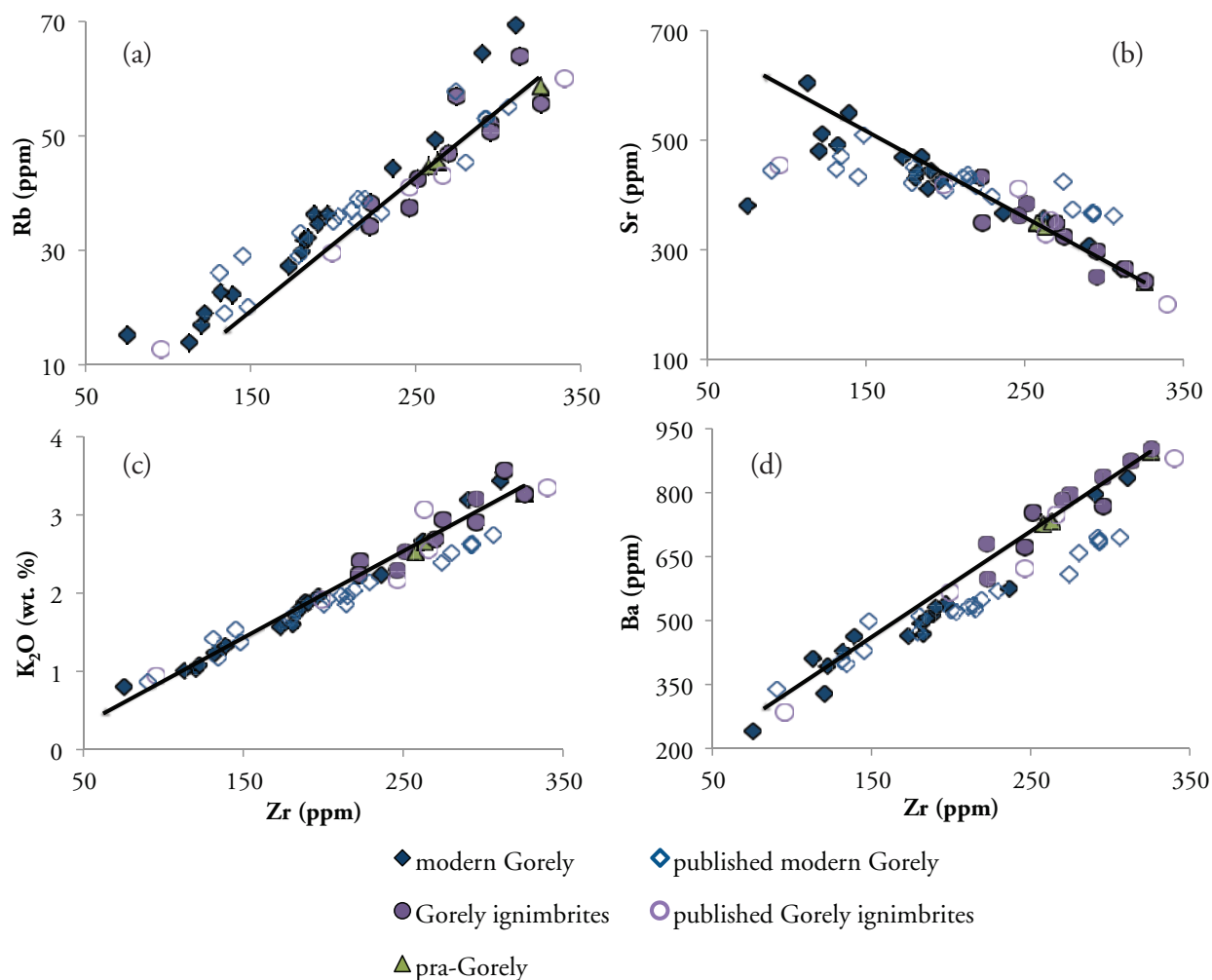
Fig. 9. Variation of Rb (a), Sr (b), K_2O (c) and Ba (d) versus the incompatible trace element Zr. The black lines are linear trends through the Gorely dacites, which point back to a possible initial magma composition. Error bars are smaller than the symbol size. Data are from this study and Kepezhinskas *et al.* (1997), Ishikawa *et al.* (2001) and Duggen *et al.* (2007).

We also used the two-pyroxene thermobarometer of Putirka (2008), which provides temperature and pressure uncertainties of $\pm 56°C$ and ± 3.7 kbar respectively (Table 6). Pyroxene chemistry was determined on five ignimbrite units, but coexisting pyroxenes (orthopyroxene and clinopyroxene) were found in only four of them (Table 4). Unit 109L-2010 provided two temperatures that met the equilibrium requirement of a K_D (based on Fe–Mg exchange) between 0.95 and 1.23. The average temperature for 109L-2010 is $926°C$ ($\pm 5°C$ 1SD) at an average pressure of 5 kbar (± 0.8 kbar). 107L-2010 yielded 11 temperature estimates, which average $891°C$ ($\pm 8°C$) at a pressure 6 kbar (± 1.1 kbar). Both temperatures determined by pyroxene thermometry are over $100°C$ lower than those determined by $\Delta^{18}O_{plag–pyx}$ (Table 6), which can be explained by slight $\Delta^{18}O$ disequilibrium between pyroxene and plagioclase grains through recycling.

DISCUSSION

Closed-system fractional crystallization using MELTS

Shallow differentiation

MELTS (Ghiorso & Sack, 1995; Asimow & Ghiorso, 1998) modeling was conducted in an attempt to obtain the liquid line of descent for the Gorely magmas, and to test if it is possible to generate dacites through fractional crystallization of basalt (Figs 11 and 12; Supplementary Data Table A3). A realistic water concentration for the parental basalt of ~ 1 wt % was used, which provided the best fit. The starting composition chosen was based on a Gorely basalt from Duggen *et al.* (2007) (Supplementary Data Table A3). The major element composition was varied within reasonable limits (within $\sim 10\%$) until a best possible fit to the dacitic composition was found. MELTS modeling shows that only at shallow conditions [1 kbar,

Table 4: Pyroxene mineral chemistry

	Notes	cpx/opx	n	SiO$_2$	TiO$_2$	Al$_2$O$_3$	FeO*	MnO	MgO	CaO	Na$_2$O	K$_2$O	Cr$_2$O$_3$	P$_2$O$_5$
109L-2010	s.c.	opx	2	53·0	0·24	0·50	18·4	1·57	23·9	1·50	0·07	0·01	0·01	0·00
	s.c.	opx	2	53·5	0·3	0·6	17·3	1·0	24·9	1·8	0·0	0·0	0·0	0·0
	s.c.	cpx	2	51·2	0·7	2·6	8·4	0·3	15·5	21·8	0·4	0·0	0·0	0·1
	s.c.	cpx	2	51·3	0·6	1·6	9·8	0·9	14·6	21·5	0·4	0·0	0·0	0·1
	s.c.	cpx	2	51·7	0·6	1·8	9·1	0·6	15·3	20·4	0·4	0·0	0·0	0·1
125L-2000	s.c.	opx	2	53·1	0·3	0·3	17·5	1·4	24·4	1·6	0·0	0·0	0·0	0·0
	s.c.	opx	2	53·0	0·3	0·7	17·5	1·4	23·7	1·7	0·0	0·0	0·0	0·0
	s.c.	opx	2	53·0	0·4	0·8	18·0	1·4	24·3	1·6	0·0	0·0	0·0	0·0
	s.c.	opx	2	53·3	0·3	0·8	18·0	1·3	24·4	1·7	0·0	0·0	0·0	0·0
	s.c.	cpx	2	51·9	0·5	1·4	8·6	0·8	15·0	21·8	0·4	0·0	0·0	0·1
77L-144	s.c.	opx	2	53·4	0·3	0·7	18·0	1·6	24·5	1·4	0·0	0·0	0·0	0·0
	agg. 1	opx	2	53·0	0·5	1·5	16·6	0·9	25·1	2·0	0·0	0·0	0·0	0·0
	agg. 2	opx	2	53·4	0·3	0·6	18·2	1·5	24·3	1·4	0·0	0·0	0·0	0·0
	s.c.	opx	2	53·6	0·2	0·5	18·0	1·0	24·4	1·4	0·0	0·0	0·0	0·0
11G-2	s.c.	opx	2	53·4	0·3	1·0	17·4	0·9	24·9	1·8	0·0	0·0	0·0	0·0
	agg. 1	opx	2	51·9	0·5	0·9	22·1	0·9	21·0	2·1	0·0	0·0	0·0	0·0
	s.c.	cpx	2	52·3	0·5	1·4	9·2	0·8	15·5	20·3	0·4	0·0	0·0	0·1
	agg. 1	cpx	2	52·1	0·6	1·4	9·2	0·8	15·0	20·9	0·4	0·0	0·0	0·1
108L-2010	m.e.	opx	2	53·2	0·2	0·8	18·1	1·3	24·0	1·5	0·0	0·0	0·0	0·0
	s.c.	cpx	2	52·0	0·5	1·4	10·6	0·9	14·2	20·1	0·4	0·0	0·0	0·1
	s.c.	cpx	2	51·3	0·7	2·4	8·9	0·4	15·5	20·1	0·3	0·0	0·0	0·1
107L-2010	s.c.	opx	2	53·9	0·3	0·7	16·6	1·4	25·6	1·4	0·0	0·0	0·0	0·0
	s.c.	opx	2	54·2	0·3	0·7	16·5	1·4	25·9	1·4	0·0	0·0	0·0	0·0
	s.c.	opx	2	53·4	0·3	0·9	16·8	1·6	25·1	1·5	0·0	0·0	0·0	0·0
	s.c.	cpx	2	52·1	0·4	1·3	10·4	0·9	14·5	20·1	0·3	0·0	0·0	0·1

n, number of analyses; s.c., single crystal; agg., aggregate; m.e., mafic enclave; opx, orthopyroxene; cpx, clinopyroxene.
*Total iron given as FeO.

Table 5: Plagioclase mineral chemistry

	Notes	An content	SiO$_2$	TiO$_2$	Al$_2$O$_3$	FeO	MnO	MgO	CaO	Na$_2$O	K$_2$O	P$_2$O$_5$
109L-2010		42·2	57·1	0·07	26·9	0·49	0·00	0·05	8·02	7·05	0·32	0·03
125L-2000		43·4	57·6	0·05	26·7	0·49	0·00	0·05	8·50	6·92	0·44	0·02
77L-144		47·8	55·5	0·05	26·8	0·59	0·01	0·06	10·2	6·92	0·30	0·02
11G-2	aggregate	47·7	56·7	0·05	27·6	0·61	0·02	0·06	9·45	6·75	0·35	0·04
108L-2010		35·3	59·1	0·00	25·3	0·43	0·00	0·04	7·42	8·02	0·48	0·03
107L-2010		40·2	57·0	0·06	25·0	0·42	0·00	0·05	8·60	6·74	0·34	0·03

nickel–nickel oxide (NNO) oxygen fugacity] is a Gorely basalt broadly capable of producing the Gorely dacites, which requires 60–75% fractionation and constitutes ~25–40% of the original magma (Fig. 11). Even though our two-pyroxene data suggest differentiation at higher pressure, modeling at 5–6 kbar gave significantly different trends from that displayed by the Gorely magmas for most major elements (Fig. 12). Varying the oxygen fugacity to quartz–fayalite–magnetite (QFM) and QFM + 2 generated a slightly better fit to the data for some elements, but

Table 6: Sr–Nd–O isotope compositions and thermometry results of Gorely eruptive products

Sample no.	$\delta^{18}O_{plag}$	2σ	$\delta^{18}O_{cpx}$	2σ	$\delta^{18}O_{gm}$	2σ	$\delta^{18}O_{melt}$ Plag*	SE
07L-53	5·57	0·10	4·68	0·08			6·41	0·09
07L-54	5·73	0·11					6·02	0·09
107L-2010	5·44	0·02	4·81	0·11			5·78	0·09
108L-2010	5·54	0·11	4·89	0·11			5·77	0·09
109L-2010	5·30	0·11	4·57	0·12			5·56	0·09
11G-1	5·18	0·07	4·37	0·05			5·57	0·06
11G-10	5·65	0·11	4·97	0·12			5·90	0·06
11G-12	6·09	0·13					6·09	0·06
11G-13	5·84	0·07	5·13	0·04			5·91	0·04
11G-14	5·89	0·08	4·96	0·08			6·22	0·04
11G-15	5·25	0·08	4·10	0·06			5·64	0·06
11G-16	5·20	0·09	4·55	0·07			5·40	0·06
11G-17	5·40	0·05	4·89	0·06			5·47	0·06
11G-18	5·71	0·02	5·23	0·05			5·38	0·06
11G-19	6·18	0·08	5·13	0·06			6·14	0·04
11G-2	5·19	0·09					5·55	0·06
11G-20	6·08	0·11	5·15	0·06			6·12	0·04
11G-21	5·59	0·12	4·85	0·05			5·68	0·04
11G-23	5·76	0·12	4·96	0·05			5·79	0·04
11G-24	5·88	0·11	5·06	0·11			5·96	0·40
11G-3a†	5·71	0·16	4·89	0·07			6·07	0·06
11G-3b†	5·69	0·12	4·62	0·06			6·04	0·06
11G-4	6·04	0·12	5·16	0·09			6·11	0·06
11G-5					5·9	0·10		
11G-6	5·10	0·02					5·41	0·06
11G-7	6·07	0·10					6·08	0·04
11G-8	5·71	0·11					5·69	0·04
11G-9	5·95	0·09	4·94	0·09			5·96	0·04
125L-2000	4·99	0·09	4·33	0·08			5·32	0·09
2005L-19	4·53	0·10	3·79	0·06			4·85	0·09
77L-144	5·77	0·08	5·08	0·09			5·84	0·09

Sample no.	$\delta^{18}O_{melt}$ CPX*	SE	$\Delta^{18}O_{pyx-plag}$ T (°C)	$^{87}Sr/^{86}Sr$	2σ	$^{143}Nd/^{144}Nd$	2σ
07L-53	5·9	0·10	980				
107L-2010	6·13	0·10	1190	0·70328	0·00001	0·513046	0·00001
108L-2010	5·96	0·09	1190				
109L-2010	5·71	0·10	1100‡	0·70332	0·00001	0·513074	0·00001
11G-1	5·80	0·10	1020§	0·70351	0·00001	0·513025	0·00001
11G-10	6·83	0·06	1150				
11G-13	5·85	0·06	1010				
11G-14	6·25	0·07	930				
11G-15	5·54	0·07	820				
11G-16	5·56	0·06	1130				
11G-17	5·60	0·06	1200				
11G-18	5·87	0·06	1250				

(continued)

Table 6: Continued

Sample no.	$\delta^{18}O_{melt}$ CPX*	SE	$\Delta^{18}O_{pyx-plag}$ T (°C)	$^{87}Sr/^{86}Sr$	2σ	$^{143}Nd/^{144}Nd$	2σ
11G-19	5·59	0·07	760				
11G-20	5·79	0·06	820				
11G-21	5·61	0·06	975				
11G-23	5·57	0·07	910				
11G-24	5·80	0·06	900				
11G-3a†	6·25	0·06	1020				
11G-3b†	5·98	0·07	870				
11G-4	5·87	0·06	890				
11G-9	5·51	0·07	780				
125L-2000	5·62	0·10	1150				
2005L-19	5·07	0·07	1050	0·70343	0·00001	0·513093	0·00002
77L-144	6·24	0·10	1130	0·70335	0·00001	0·513035	0·00001

$\delta^{18}O$ values are per mil deviations from VSMOW.
*$\delta^{18}O_{melt}$ values were calculated from the pyroxene and plagioclase phenocryst $\delta^{18}O$ values based on known fractionation factors between the mineral and melt at known SiO_2 concentrations (Bindeman *et al.*, 2004).
†11G-3a and 11G-3b are two pumice clasts from the same eruption.
‡109L-2010 reported a 2-pyx (Putirka, 2008) temperature of $926 \pm 5·2$°C (1SD) based on two analyses.
§11G-1 reported a 2-pyx (Putirka, 2008) temperature of $891 \pm 8·0$°C (1SD) based on 12 analyses.
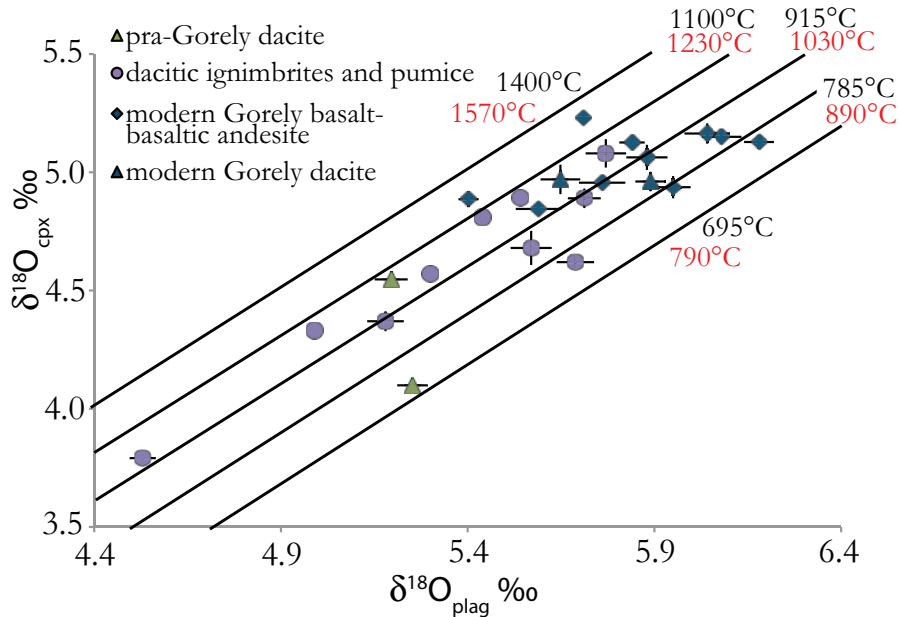
Fig. 10. Variation of $\delta^{18}O_{plag}$ vs $\delta^{18}O_{cpx}$ for the Gorely magmatic rocks ($\pm 2\sigma$). Also shown are $\Delta^{18}O_{plag-cpx}$ equilibrium temperature ranges for basalts from modern Gorely (black) and dacites from both the ignimbrites and pra-Gorely sequence (red), based on the isotope fractionation thermometer of Chiba *et al.* (1989), and using An43 (dacites) and An65 (basalts). Contours are calculated by holding the temperature and An content constant in the Chiba *et al.* (1989) thermometer and varying the $\Delta^{18}O_{plag-cpx}$ (see text for discussion).

caused the trend to be very different for others (Fig. 12). Based on the best-fit conditions, MELTS yields a liquidus temperature of ~1240°C. However, even through a 'best-run' MELTS model does not fit the Gorely data well for TiO_2, P_2O_5, CaO, or the alkalis, perhaps due to variations in pressure, H_2O concentration, and oxidation state.
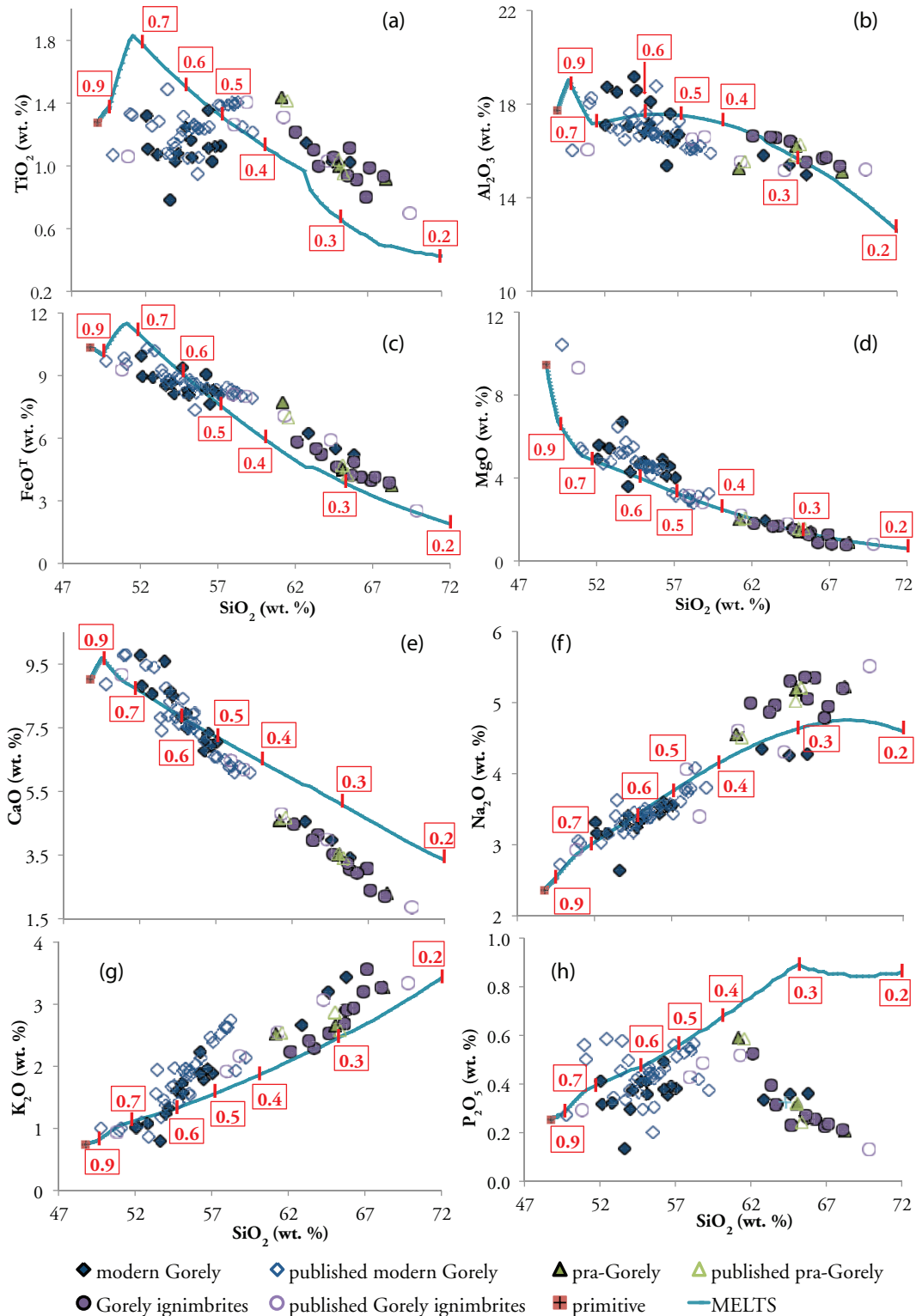
Fig. 11. Major element MELTS modeling of Gorely basaltic magmas to produce dacitic compositions through fractional crystallization. MELTS parameters are 1 kbar pressure, NNO oxygen fugacity, and a liquidus temperature of ~1240°C. The MELTS trends overlap with the evolved compositions reasonably well for most major oxides, except for offsets in TiO_2, P_2O_5, CaO, and the alkalis (see text for discussion). MELTS modeling at higher pressure (including two-stage modeling from 5 to 1 kbar) or lower oxygen fugacities does not fit the data (see Fig. 12). Data sources are listed in the Fig. 6 caption.
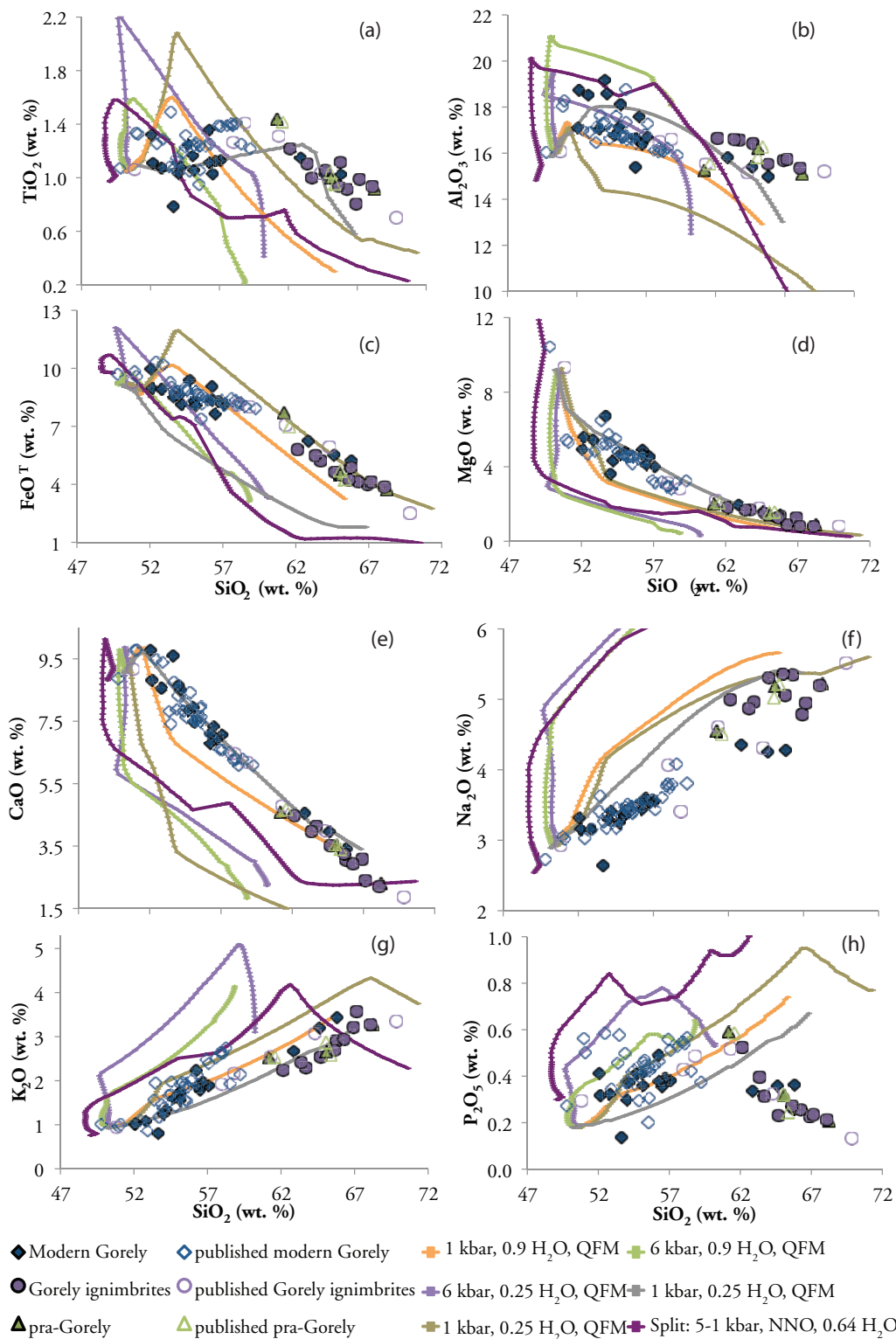
Fig. 12. MELTS modeling at varying pressure, melt water content, and oxygen fugacity. The split run was carried out at 5 kbar for the basalts, and then switched to 1 kbar at 55 wt % SiO2. These runs clearly show that crystallization at higher pressure, or lower oxygen fugacity or water content cannot produce the evolved Gorely compositions.

These changes would cause the timing for multiple mineral saturation (i.e. apatite, plagioclase, Fe–Ti oxides) to vary. Another possible reason for these discrepancies could be that the calibration of apatite crystallization and plagioclase composition in MELTS is not yet sufficient.

Deep differentiation

Shallow differentiation has been partially challenged by Gavrilenko & Ozerov (2010), who suggested a two-stage differentiation model for the Gorely magmas, similar to that proposed by Annen et al. (2006), in which there is an early state of high-pressure differentiation at 6–8 kbar and a second stage of differentiation at 1–1·5 kbar. Therefore, we also attempted a two-stage differentiation model using MELTS, but the trend still did not fit our data (Fig. 12). For all elements, the fits worsen owing to early crystallization of pyroxene at higher pressure. This causes an early, strong, decrease in MgO and CaO, which does not follow the Gorely trend. In addition, it causes all other elements to increase steeply at low SiO_2 for the Gorely magmas. This causes any differentiation at depth (including the two-stage differentiation) not to overlap with either the mafic or evolved Gorely magmas, even when H_2O content and oxidation state are varied (Fig. 12). These results do not preclude minor refills of deep, differentiated magma, which may contain some pyroxene, but they do show that the primary chemical makeup of the magma was achieved at shallow depths, which is supported by our $\delta^{18}O$ results below.

Daly Gap, low-$\delta^{18}O$ magmas, and the relative roles of fractional crystallization and crustal melting

MELTS modeling suggests that it is compositionally difficult but possible to produce the evolved compositions of the ignimbrite units by 60–75% fractional crystallization of large quantities of basalt. Another indication of the need for a process besides just fractional crystallization to produce these dacites is the clear preponderance of silicic rocks and the bimodality of volcanism at the Gorely eruptive center, which represents an unmistakable Daly Gap (Fig. 6). It is important to note that this trend is probably not due to a sampling bias, as we included all data on Gorely magmas from the GEOROC database. The origin of the Daly Gap (Daly, 1925; Chayes, 1963) in volcanic suites has been debated for decades. The Daly Gap may reflect derivation of the magmas from multiple, chemically distinct reservoirs (e.g. mantle, crustal, or residual mushes), or through the physics of crystal retention following fractional crystallization (Chayes, 1963; Marsh, 1981; Brophy, 1991; Grove et al., 1997; Thompson et al., 2002; Dufek & Bachmann, 2010; Czuppon et al., 2012), or it may be a natural side effect of fractional crystallization, as magmas of intermediate composition may actually be formed through 'mingling and mixing' (Reubi & Blundy,

2009). More recently, Dufek & Bachmann (2010) suggested mechanical ways to produce a Daly Gap through retention of crystal mushes of intermediate composition, which suggests that the 'missing' andesites may still be located at greater depths. Those researchers suggested that liquid–crystal separation occurs most efficiently at crystallinities of ∼50–70 vol. % (the 'extraction window'). This range encompasses the 60–75% crystallization needed to form the Gorely dacites (according to MELTS modeling). Deering et al. (2011, 2012) used such an 'extraction window' to show that compositional offsets, which we also observe, can be produced through a change in the depth of differentiation or a change in oxygen fugacity, and a subsequent change in the liquid line of descent, without the need for crustal assimilation. Furthermore, Melekhova et al. (2013) suggested that magmas with high H_2O concentrations (and lower temperatures) are more likely to produce a Daly Gap via amphibole influence on SiO_2, and thus strictly through fractional crystallization; this may pertain to the Gorely magmas, as a few units contain amphibole, although most are amphibole-undersaturated. This is similar to the work of Grove & Donnelly-Nolan (1986), who suggested that differentiation over a large compositional range but over a small temperature range might aid in the formation of a Daly Gap. However, although the Daly Gap in the Gorely data may in theory be produced by arbitrary choices of polybaric liquid lines of descent, variations in intensive parameters (oxygen fugacity, H_2O concentration), the presence of amphibole and mechanics of extraction, the trace element trends described above and the isotopic diversity that we observe in the Gorely ignimbrites require diverse sources and processes.

One line of evidence against strictly isobaric fractional crystallization is the separate trends shown in the Harker diagrams for K_2O, Rb, Ba, and Sr (Figs 8 and 9). This offset must be due to one of three processes: (1) crystallization of the basalts at a different depth compared with the dacites; (2) the 'extraction window' processes described by Dufek & Bachmann (2010); (3) assimilation of crustal rocks that are lower in K_2O, Ba and Rb and enriched in Sr. Deering et al. (2011) showed that offsets in Rb and K_2O can be produced through fractional crystallization using the 'extraction window' of crystal mushes proposed by Dufek & Bachmann (2010), along with variations in differentiation depth. Although this method may have worked for Deering et al. (2011), their data do not show the isotopic variations that our data show, and differentiation of the Gorely basalts at a higher pressure in the presence of amphibole is only capable of producing dacites with lower Rb concentrations. This is not possible for Ba or K_2O, and the trend is opposite for Sr. This is because bulk partition coefficients of a cumulate assemblage changing from amphibole-free to amphibole-bearing when fractionating from basalt (50% pyroxene, 50% plagioclase) to

dacite (30% amphibole, 35% plagioclase, 35% pyroxene) are not greater than unity. For amphibole in dacite, partition coefficients (D) are 0·28 (Ba), 0·18 (Rb), 0·081 (K), and 0·6 (Sr), whereas plagioclase D values in dacite are 0·3 (Ba), 0·24 (Rb), 0·1 (K), and 4·4 (Sr). D values for plagioclase in basalt are 0·2 (K), 0·067 (Rb), 0·7 (Ba), and 3·08 (Sr). A realistic D for Sr in clinopyroxene is ∼0·11, and nearly 0·0 for Rb, K, and Ba (Onuma *et al.*, 1968; Nagasawa & Schnetzler, 1971; Ewart & Griffin, 1994; Bindeman *et al.*, 1998). Furthermore, the similar slopes for the basalt–basaltic andesites and andesite–dacites on the Harker variation diagrams suggest that the bulk partition coefficients were either the same or similar. An increase in compatibility of these elements (e.g. Rb in a hypothetical amphibole-rich dacite) would cause a change in slope (making it more shallow, but continuous), but would not create a jump similar to what we see (Figs 8 and 9). Therefore, this method of melt extraction is not capable of producing the offset trends that we see in our data, and a different process must be occurring.

The strongest argument against a single evolving magmatic series, or a single evolving crystal mush, is that based on the isotopic heterogeneity. The low $\delta^{18}O$ and $^{143}Nd/^{144}Nd$ values, and high $^{87}Sr/^{86}Sr$ determined in this study suggest the involvement of a variety of crustal assimilants. The oxygen isotope data suggest periodic melting and assimilation of hydrothermally altered, low-$\delta^{18}O$ material into the Gorely magmatic system. Although crustal melting and differentiation have probably occurred at different depths for some basalts or dacites, shallow crustal assimilation must be a near-ubiquitous, pre-eruptive process in order to imprint and preserve this low-$\delta^{18}O$ signature in some eruptive products. This is shown in the six units erupted from Gorely that have a $\delta^{18}O_{melt}$ below the mid-ocean ridge basalt (MORB) value of $5·7 \pm 0·2$‰ (Table 6; Fig. 5b).

Other magmatic rocks, including most of the Holocene basalts and basaltic andesites from the modern Gorely stratocone, are normal in $\delta^{18}O$ (>5·7‰), and their $\delta^{18}O$ variations may be explained by 10–50% fractional crystallization of normal $\delta^{18}O$, mantle-derived basalt (Fig. 11). However, even normal $\delta^{18}O$ values do not necessarily preclude assimilation of normal $\delta^{18}O$ hydrothermally altered materials, which could still alter the magma's major element composition. Hydrothermal alteration by −14‰ meteoric water at low to moderate temperature, with $\Delta^{18}O_{rock–water}$ of ∼19‰, leads to a nil isotopic effect. This same nil effect is also characteristic for hot, but isotopically shifted meteoric waters that have interacted and equilibrated with enough rocks upstream. This would cause the $\delta^{18}O$ of the water to have already shifted to higher values, which would cause the water to have no effect on the $\delta^{18}O$ of the rocks it interacted with later (i.e. the normal $\delta^{18}O$ rocks of Gorely). Six dacite units, including two

ignimbrites (11G-1/2, 108L-2010), have normal $\delta^{18}O$ values >5·7‰. In addition, the higher $^{87}Sr/^{86}Sr$ and lower $^{144}Nd/^{143}Nd$ and $\delta^{18}O$ values for the remaining dacitic ignimbrites, lavas and tephra, and their variation with time, are consistent with periodic shallow assimilation of hydrothermally altered crust, which we explore in the following sections.

Potential crustal contributions to Gorely magmas

Because the currently oldest known ignimbrite of 361 ka (2005L-19) erupted from the Gorely magmatic system has the lowest $\delta^{18}O$ value, the system could have assimilated older surrounding crust (basement) that was already hydrothermally altered. Sources of underlying material that might affect the composition of the Gorely magmas include the Late Miocene Akhomten Granite Massif, ∼2–1·5 Ma rhyolitic ignimbrites extruded (or remaining) from the nearby Karymshina caldera, the nearby 4 Ma ignimbrites from this study, and silicic material from the neighboring stratovolcanoes Opala, Karymshina, Zhirovskoy and Mutnovsky or their subvolcanic plumbing systems (Figs 1, 7 and 13). Additionally, there could be earlier, now buried, unknown Gorely ignimbrite eruptions prior to 2005L-19 (Figs 1 and 2; Bindeman *et al.*, 2010). These could have experienced hydrothermal alteration during pra-Gorely magmatism, and were later assimilated back into the magmatic system through a series of caldera collapses, thereby lowering the $\delta^{18}O$ of the magma that was later erupted (as unit 2005L-19). This is similar to the interpretation proposed for low-$\delta^{18}O$ Yellowstone magmas (Bindeman *et al.*, 2001). We use $^{87}Sr/^{86}Sr$, $^{143}Nd/^{144}Nd$, and $\delta^{18}O$ isotopic values, and major and trace element concentrations, to identify possible sources for crustal contributions to the Gorely magmas.

The strontium and neodymium isotopic compositions of Karymshina magmas are similar to those of the Gorely eruptive center, and could produce the desired ratios through assimilation (high $^{87}Sr/^{86}Sr$, low $^{143}Nd/^{144}Nd$); however, $\delta^{18}O_{melt}$ values for the Karymshina magmas are exclusively higher than the $\delta^{18}O_{melt}$ values of the Gorely magmas, suggesting that buried Karymshina rocks must have undergone high-temperature hydrothermal alteration, and lost Rb, Ba, and K_2O, if they were to contribute to Gorely magmatism (Fig. 13).

Although Mutnovsky $^{87}Sr/^{86}Sr$ and $^{143}Nd/^{144}Nd$ values are appropriate for assimilation into the Gorely magmas (Fig. 13), and the lower K_2O content of the Mutnovsky magmas could produce the offset in K_2O of the Gorely dacites (Fig. 7), the Mutnovsky magmas are universally normal in $\delta^{18}O$ (basalts and andesites) (Bindeman *et al.*, 2004). Furthermore, as evidenced by Duggen *et al.* (2007) using double-spike Pb isotope techniques, even though Mutnovsky is only ∼10 km away from the Gorely eruptive center (Fig. 1), the Mutnovsky magmas have a separate
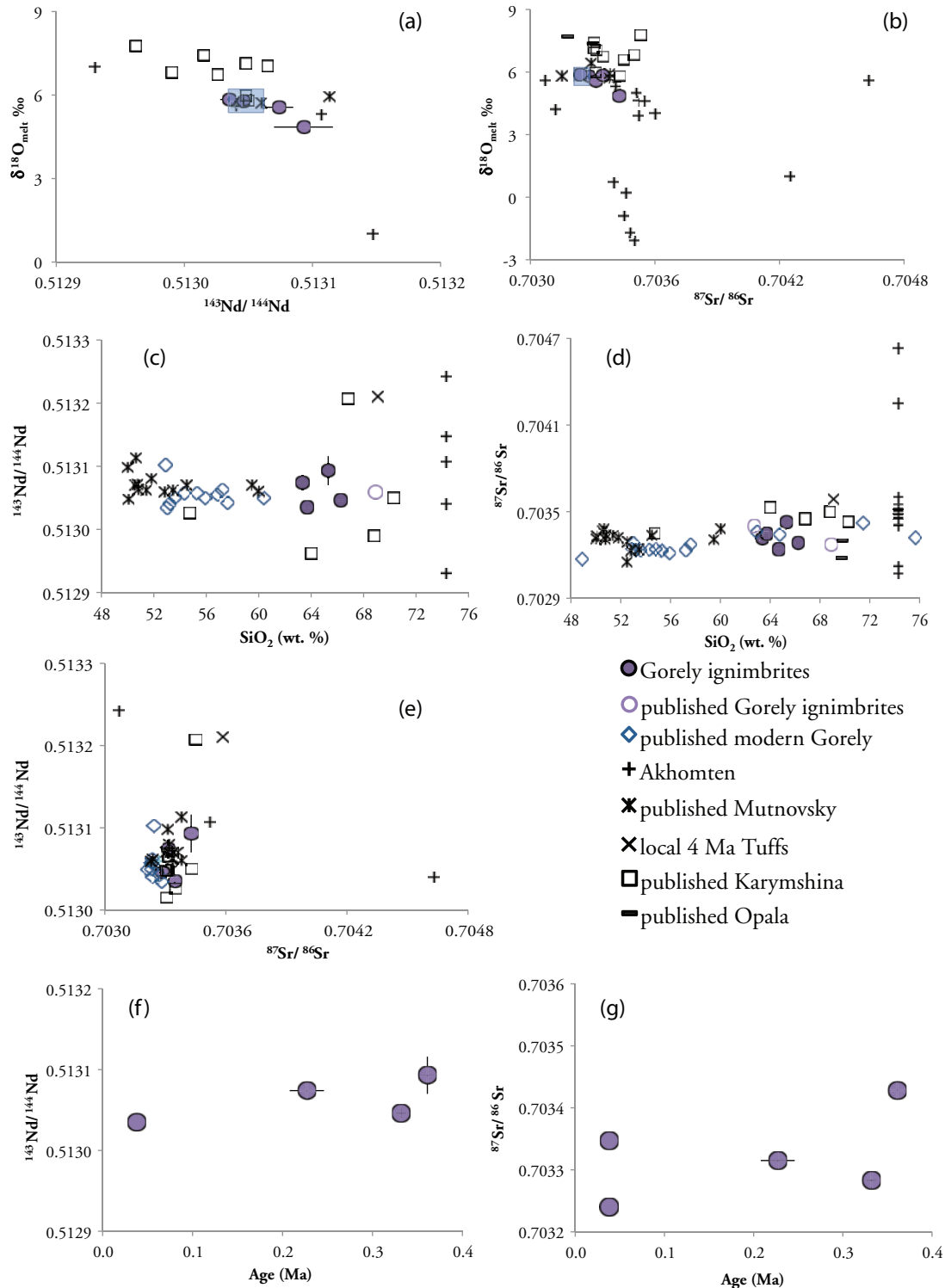
Fig. 13. (a–e) Sr–Nd–O isotope variations in Gorely silicic compositions compared with modern Gorely lavas and tephra, and silicic rocks from neighboring centers: Akhomten Massif, Opala volcano, Karymshina volcano, 4 Ma tuffs, and Mutnovsky volcano (Figs 1 and 2). The range for modern Gorely lavas and tephra is shown as a blue rectangle in the $\delta^{18}O_{melt}$ plots using $\delta^{18}O_{melt}$ calculated in this study and $^{87}Sr/^{86}Sr$ and $^{143}Nd/^{144}Nd$ data from Duggen et al. (2007). (f, g) temporal $^{143}Nd/^{144}Nd$ and $^{87}Sr/^{86}Sr$ variations in the Gorely ignimbrites. Gorely data from the literature are listed in the Fig. 6 caption in addition to Hedge & Gorshkov (1977) and Shipley (2011); data for Karymshina, Mutnovsky, and Opala are listed in the Fig. 6 caption; Akhomten Massif $\delta^{18}O$ data are from Vinogradov (1995); $\delta^{18}O$ values from the Akhomten Massif are whole-rock values; $\delta^{18}O$ values from Mutnovsky volcano are for glass. All other data are calculated melt compositions from $\delta^{18}O$ analyses on phenocrysts from this study (Table 6).

plumbing system. Earlier 300–100 ka low-δ^{18}O dacitic ignimbrites from Gorely, including those exposed in the Opasny Ravine, are thus derived from Gorely and not Mutnovsky, and did not assimilate Mutnovsky material during their production. In addition, Opala, which is ~58 km west of Gorely, is unlikely to share a magma plumbing system, owing to its high δ^{18}O signature (Bindeman *et al.*, 2004). Moreover, the isotopic data from this study show that the ^{143}Nd/^{144}Nd of the 4 Ma tuffs is too high to produce the low ^{143}Nd/^{144}Nd of the Gorely magmas. Zhirovskoy, a nearby, eroded volcano, is made of basalts to basaltic andesites and is not yet isotopically characterized.

The Akhomten Granite Massif of Miocene age, proximal to Gorely (Figs 1 and 2), has yielded a whole-rock Rb–Sr isochron age of 12·5 ± 0·8 Ma (Vinogradov, 1995), which is largely confirmed by a U–Pb zircon crystallization age of 11·2 ± 0·08 Ma (1SE) from this study (Supplementary Data: Table A1). This massif is characterized by a wide range of ^{87}Sr/^{86}Sr and ^{143}Nd/^{144}Nd (0·70307–0·70463 and 0·51293–0·513242 respectively), and importantly, has low and variable Rb, and high and variable Sr contents (Vinogradov, 1995), largely reflecting a diverse crustal source. Most importantly, the massif is characterized by a wide range of δ^{18}O values, with many rocks exhibiting low δ^{18}O values (Fig. 13), all of which overlap with, or are lower than, Gorely isotopic values. It is not known whether the Akhomten Massif developed low δ^{18}O values upon its emplacement, or whether Quaternary volcanic activity has been imprinted on it. Given the age of the Akhomten Massif, it is probably associated with the timing of collision of the Kronotski block with Kamchatka between 10 and 5 Ma (Lander & Shapiro, 2007), suggesting that the Akhomten Massif may be sourced from the Kronotski block. The xenocrystic zircon that we found (37·5 ± 0·7 Ma rim probably metamorphic owing to its low Th/U ratio and 54·7 ± 1·1 Ma core) suggests that the assimilated crustal rocks might have included the older basement of the Achaivayam–Valaginsky Arc, which forms much of the basement under eastern Kamchatka and was accreted between 45 and 50 Ma. The Akhomten Massif may underlie Gorely (Fig. 1) and thus may have been assimilated by the Gorely dacites, giving them their isotopic diversity and low δ^{18}O signature (Fig. 13). Similar conclusions for diverse δ^{18}O assimilants were reached by Weismaier *et al.*, (2012) for Teide in the Canary Islands. We thus used Akhomten as the most likely end-member in energy-constrained assimilation-fractional crystallization (EC-AFC) modeling.

EC-AFC as a means to determine the source for assimilation
EC-AFC (Bohrson & Spera, 2001; Spera & Bohrson, 2001) was used to determine if, chemically and isotopically, which country rocks could be a plausible source for assimilation by the Gorely magmas. We found that the Akhomten Massif is the most probable source (Fig. 14;

Supplementary Data: Fig. A8). For the thermal set-up and equilibration parameters we used the liquidus temperature determined by MELTS modeling discussed above (1240°C) and an initial temperature of the assimilant of 500°C, which is appropriate for the middle crust or pre-heated upper crust. Lower temperatures did not achieve the assimilation needed in terms of the isotopic ratios (δ^{18}O, ^{87}Sr/^{86}Sr, and ^{143}Nd/^{144}Nd) to produce the dacitic composition of the ignimbrite. This implies the need for a previously heated system prior to the initiation of assimilation, with an equilibration temperature of ~1000°C. We left all other values the same as those suggested by Bohrson & Spera (2001) for the 'standard, nonlinear, upper-crustal case'. Modeling was based on the Sr, Nd, and O isotope ratios, and Sr and Nd compositions of the mafic and dacitic Gorely magmas and the Akhomten Massif (Supplementary Data: Tables A4–A7).

We ran four models to quantify the degree of assimilation: (1) the assimilation of the average Akhomten Massif; (2) the assimilation of the first erupted Gorely ignimbrite (2005L-19; 361 ka); (3) a low ^{143}Nd/^{144}Nd assimilant; (4) reverse modeling to determine the isotopic end-member by using the best fit of isotopic ratios and concentrations to achieve the ignimbrite compositions. We used recharge only in the best-fit run and kept the recharge composition the same as that of the initial magma (Sr and Nd concentrations, as well as Sr, Nd, and O isotopic ratios similar to those of Gorely basalts). Details for these runs are listed in Supplementary Data Tables A4–A7.

The best-fit model is the only one that achieved a high enough ^{143}Nd/^{144}Nd for the ignimbrite compositions. This clearly demonstrates that a higher ^{143}Nd/^{144}Nd ratio is needed than that of the first known ignimbrite erupted (2005L-19), or of the average Akhomten Massif, but not necessarily higher than what is seen in the Akhomten Massif. This is in contrast to the ^{87}Sr/^{86}Sr, which was easily achieved by all model runs. In terms of δ^{18}O, all runs achieved a reasonable δ^{18}O for the ignimbrites using the realistic (and low, 3–4‰) range of δ^{18}O in Akhomten. Given the large isotopic heterogeneity of the Akhomten Massif (standard deviations of 2·81, 0·000378, and 0·0001169 and values in the range of 10–7·0‰, 0·70307–0·70463, and 0·512930–0·513242 for δ^{18}O, ^{87}Sr/^{86}Sr, and ^{143}Nd/^{144}Nd, respectively) this is not surprising.

One curious result of this modeling is the need for rather high ^{87}Sr/^{86}Sr in relation to the high (not low) ^{143}Nd/^{144}Nd of the assimilant to produce the Gorely ignimbrites. The high ^{87}Sr/^{86}Sr and variable nature of the average Akhomten Massif makes this a possible assimilant to form the Gorely ignimbrites. Therefore, we ran a fourth model in which a Gorely basalt had a higher initial ^{143}Nd/^{144}Nd, and assimilated a lower ^{143}Nd/^{144}Nd portion of the Akhomten Massif. This allowed the model to run through one of the ignimbrite samples (77L-144), and near
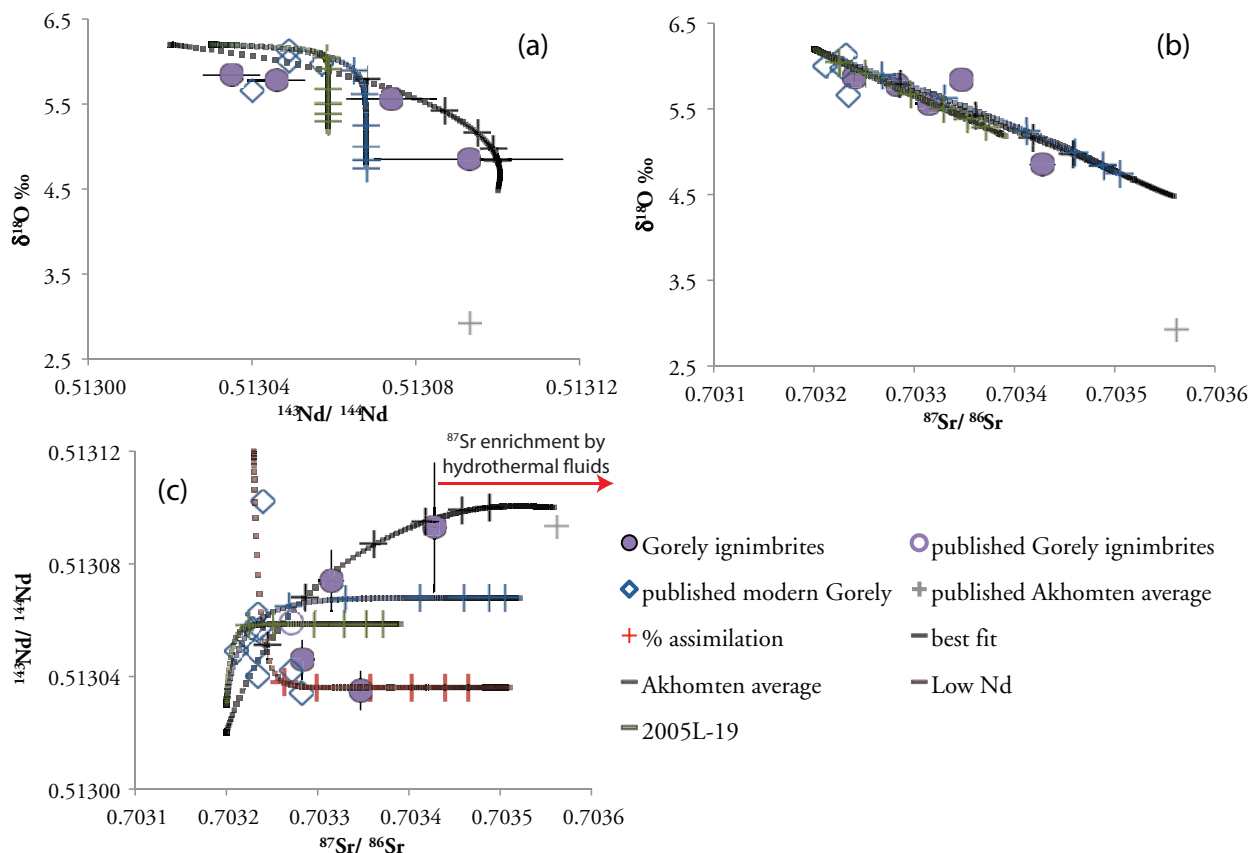
Fig. 14. EC-AFC modeling of the Gorely magmas to fit the Sr–Nd–O isotopic compositions of the ignimbrites. Four separate models are shown [best fit, average Akhomten, 2005L-19, and initial low $^{143}Nd/^{144}Nd$ (Low Nd)]. The plus signs are color coordinated with each separate model run and represent the per cent assimilation (5, 10, 20, 30, 40, and 50). Gorely literature data are from Kepezhinskas *et al.* (1997) and Duggen *et al.* (2007), and Akhomten data are from Vinogradov (1995).

another (107L-2010), showing that it is possible that not all ignimbrite units were formed through a single-path assimilation process, which could be made possible through (1) the variable nature of the Akhomten Massif and (2) preferential addition of radiogenic Sr through hydrothermal alteration.

Hydrothermal fluids emanating near the Gorely volcanic center (from Zhirovskoy, Mutnovsky, and Opala) have $^{87}Sr/^{86}Sr$ ranging from 0·70349 to 0·70429 (Vinogradov & Vakin, 1983), which are all higher than the highest $^{87}Sr/^{86}Sr$ observed at Gorely (0·70343). Through hydrothermal circulation, these high $^{87}Sr/^{86}Sr$ values may be the source of the two high $^{87}Sr/^{86}Sr$ ignimbrites (2005-Ll9 and 109L-2010), which could have retained excess Sr, with a higher $^{87}Sr/^{86}Sr$ ratio, leached from the Cretaceous crust. This would probably be caused by precipitation of alunite (e.g. John *et al.*, 2008), which is a strontium-rich mineral commonly found in hydrothermal systems. Assimilation of this type of material could explain the high Sr (348 ppm) and high $^{87}Sr/^{86}Sr$ we see in these two Gorely ignimbrites. A negative correlation of

$^{87}Sr/^{86}Sr$ and $\delta^{18}O$ for silicic rocks across Kamchatka (Bindeman *et al.*, 2004) supports this interpretation (Fig. 13).

According to the EC-AFC modeling conducted here, *c.* 15% assimilation is needed to produce 109L-2010 (dacite ignimbrite), and *c.* 30% assimilation to produce 2005-Ll9 (dacite ignimbrite). These numbers would increase if the parameters in the EC-AFC model were changed, such as if the liquidus temperature or initial temperature of the assimilant were decreased. Therefore other components, such as recharge, would probably need to be added to achieve this greater amount of assimilation and melting.

Although trace elements were not included in the EC-AFC modeling, we nevertheless show that portions of the Akhomten Massif have the Rb and Sr concentrations needed to produce the offsets observed in the Gorely magmas (Figs 8 and 9). This is shown in the large range in Rb and Sr concentrations throughout the Massif, many of which are lower in Rb and elevated in Sr (Vinogradov, 1995).

Temporal evolution of Gorely magmatism: evidence through petrography and isotopes

The large range in the isotopic signatures of the Gorely magmas described above provides strong evidence for assimilation of a crustal source (the Akhomten Massif) that could imprint its $^{87}Sr/^{86}Sr$, $^{144}Nd/^{143}Nd$, and $\delta^{18}O$ values through the combined effects of assimilation–fractional crystallization and hydrothermal alteration, but also has the ability to repeatedly produce the geochemically and mineralogically similar dacitic compositions observed through the early evolution of the Gorely eruptive center (Figs 5 and 13).

The decrease in isotopic diversity of the Gorely magmas with decreasing age and the increasing predominance of normal $\delta^{18}O$ values may indicate that after tens to hundreds of thousand years of 'waxing', the magmatic plumbing system under Gorely became less prone to assimilation (Fig. 5). Alternatively, the magma plumbing system may now tap more 'normal' or by now laterally averaged crustal sources with normal $\delta^{18}O$, and less diverse Sr and Nd isotopic values, owing to the low-$\delta^{18}O$ protolith being exhausted. In addition, the presence of mafic enclaves in thin sections (Table 3) and hand samples of all of these ignimbrites suggests mafic injections into the magma system at a time near the eruption, not allowing the necessary time to thoroughly mix and equilibrate this mafic material into the magmatic system prior to eruption. As was earlier documented by Sparks & Marshall (1986), and again by Izbekov *et al.* (2004*a*), the ability of magmas to thoroughly mix and re-equilibrate after a mafic injection depends primarily on the viscosity and density of the magma subsequent to thermal equilibration, followed by mechanical disintegration (mingling). As was detailed by Izbekov *et al.* (2004*a*), the presence of mafic enclaves suggests that mafic recharge was rare, owing to the need for a larger temperature and viscosity difference between the pre-existing magma and the mafic intrusion to form quenched blobs. In addition, the small degree of resorption in some of the phenocrysts contained within the mafic enclaves suggests a relatively small amount of time between mafic recharge and eruption, leaving little time for the recharge to equilibrate with the pre-existing magma.

The earliest known eruptions from Gorely include the formation of the pra-Gorely cone ($\sim$0·7 Ma). These eruptions include two low-$\delta^{18}O_{melt}$ units (Fig. 5), which suggests that either there must be earlier erupted ignimbrites, which are currently buried and not sampled, or the production of the pra-Gorely magmas must have included assimilation of hydrothermally altered surrounding crust, such as the Akhomten Massif.

Following the formation of the pra-Gorely eruptive rocks, there was an extended period of ignimbrite-forming eruptions ($\sim$360–38 ka). All but two of the ignimbrite units (108L-2010 and 109L-2010) contain glomeroporphyritic crystal aggregates (Plag + Pyx ± Mt), and these two units also contain the largest amount of mafic enclaves, with little resorption of the phenocrysts of the mafic enclaves; this suggests that mafic magma injection may have triggered convection and stirred the cumulate layers near the walls and base of the magma chamber, and that the eruption occurred within a short period of time following a mafic injection (e.g. Bergantz & Breidenthal, 2001; Izbekov *et al.*, 2004*a*). We speculate that the high $\delta^{18}O$ temperatures that we observe (Fig. 10), which are higher than the MELTS determined equilibration temperatures and the two-pyroxene temperatures, may indicate that some crystals represent 'protocrysts' [i.e. they formed early in an evolving (hotter and deeper; 5–6 kbar) magma chamber, similar to what was noted by Tollan *et al.* (2012)], or 'xenocrysts' (i.e. they were sourced from a different parent and were entrained in the 1 kbar Gorely magma system). This is documented by the abundant evidence of mixing (mafic enclaves, crystal aggregates, and sieve textures), and also by the two units 109L-2010 and 11G-2, which yielded pyroxene temperatures of 926 and 891 °C, respectively, which are over 100 °C lower than those indicated by the O isotope fractionation thermometer (1050 and 1020 °C respectively) (Table 6). As these crystals are also compositionally zoned (plagioclase has complex, normal, and reverse zoning; Table 3), and at times show sieve textures, this interpretation suggests that these crystals have not had time to equilibrate in terms of their $\delta^{18}O$ composition prior to their entrainment in a colder and more differentiated magma product, as oxygen has a slower diffusion rate than Fe and Mg in pyroxene, and we know that the pyroxenes have not been fully equilibrated (e.g. Bindeman, 2008). The final ignimbrite known to erupt before the $\sim$38 ka eruptions, 125L-2000, is also the ignimbrite with the highest percentage of crystals contained within crystal clusters (25%), suggesting that it may have erupted leftover crystal clusters from previous eruptions that remained along the walls of the magma reservoir, or that it erupted smaller pockets of leftover crystal mush, prior to a period of possible quiescence at the Gorely eruptive center (Table 3).

The next phase of ignimbrite-forming eruptions occurred between 100 and 38 ka. None of these units erupted low-$\delta^{18}O$ material. Mafic enclaves and crystal clusters were observed in thin section, suggesting a similar process of eruption triggering to the earlier ignimbrites (Table 3). Similar to the pra-Gorely temperatures, the late ignimbrite eruptions show a range of both normal and high temperatures as indicated by isotopic fractionation, although none of these units produced a reliable equilibrium temperature from the two-pyroxene thermometer. This again suggests that some crystals were entrained without enough time for equilibration (Fig. 10).

The post-38 ka cone-building phase continues to the present day. At least two small-volume Holocene (∼7 ka) units have produced low $\delta^{18}O_{melt}$ values (11G-17 and 11G-18), which probably represent sampling of lingering small pockets of low $\delta^{18}O_{melt}$ under Gorely. This post-38 ka, cone-building period of eruptions also shows a drop in SiO_2 wt % from previous eruptions (Fig. 5a), illustrating a less evolved phase even than that of the pra-Gorely period.

In summary, magmatism is temporally diverse in $\delta^{18}O$, $^{87}Sr/^{86}Sr$, $^{144}Nd/^{143}Nd$ (Figs 5b and 12f, g) and composition. This is consistent with a model whereby each magma chamber is nearly entirely emptied of melt following every ignimbrite eruption, as any significant amount of melt remaining in the chamber would not allow for such large changes in strontium and neodymium isotope composition through time. The batch of melt that produced subsequent eruptions must have had a maximum residence time of 10^3–10^5 years, based on the time spans between ignimbrite-forming eruptions, evolving through processes including fractional crystallization and assimilation of either older country rocks or hydrothermally altered crustal material (the Akhomten Massif) as observed elsewhere (e.g. Druitt et al., 2012).

Foundering of the lower crust as a source of early silicic volcanism?

It has been proposed that the 'ignimbrite flare-up' in the western USA was a consequence of the delamination of the subhorizontal Farallon slab beneath the western USA following accretion of the Siletzia Terrane (Christiansen & Yeats, 1992; Humphreys, 1995). Likewise, in Kamchatka there was a much younger episode of accretion (the Kronotski Arc) between 10 and 7 Ma (Lander & Shapiro, 2007), and an earlier episode (45–40 Ma) of accretion of the Achaivayam–Valaginsky Arc (Soloviev et al., 2002a, 2002b; Konstantinovskaya, 2003; Hourigan et al., 2009). Both of these events would have contributed to thickening of the crust beneath Kamchatka. Because Akhomten (an upper- to mid-crustal granite) has an age of only ∼11 Ma, delamination of the lower thickened crust under eastern Kamchatka would help to explain its rapid uplift and rugged topography (Fig. 3).
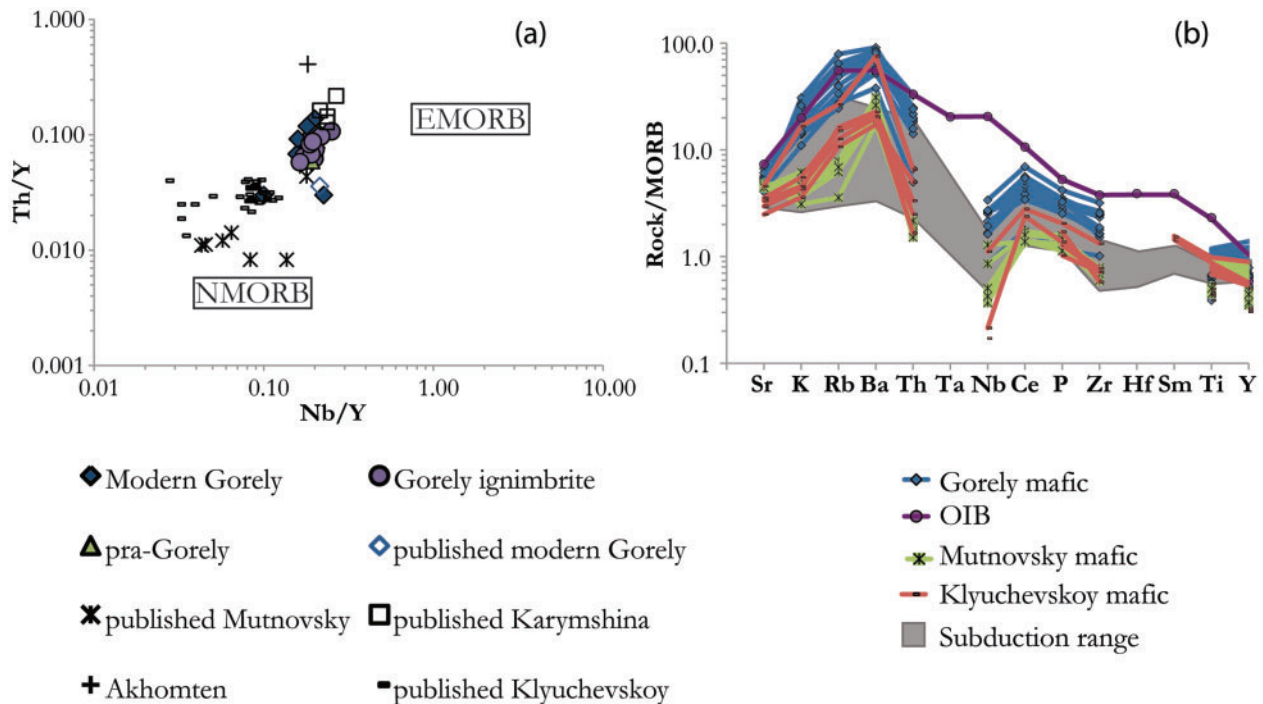
Fig. 15. Trace element variation diagrams for Gorely. (a) Th/Y vs Nb/Y, showing that Gorely basaltic magmas have higher Nb and Th concentrations than mafic magmas from Klyuchevskoy (Central Kamchatka Depression) and Mutnovsky (Volcanic Front). (b) MORB-normalized trace element patterns illustrating that the Gorely basalts have a geochemical signature between OIB and subduction-related Kamchatkan basalts. The gray field 'Subduction range' is from the Basaltic Volcanism Study Project (1981) and includes data from Sunda (tholeiitic and calc-alkaline basalt), New Zealand (high-Al basalt), the New Hebrides (high-K basalt), Java (high-Al basalt), and New Britain. Published Kamchatka data are from Kersting & Arculus (1994), Ozerov et al. (1995), Tatsumi et al. (1995), Kepezhinskas et al. (1997), Dorendorf et al. (2000), Volynets et al. (2000), Churikova et al. (2001), Ishikawa et al. (2001), Duggen et al. (2007) and Turner et al. (2007). OIB and N-MORB data are from Sun & McDonough (1989). EMORB, enriched MORB.

Block foundering and associated heating of the lower crust may help to explain the silicic explosive volcanism in southern and eastern Kamchatka (Bindeman *et al.*, 2010), as well as the elevated Nb concentrations of the Gorely magmas [average of $2 \cdot 6 \pm 0 \cdot 57$ (1SD) normalized to normal (N)-MORB] relative to typical subduction-related magmas (average of $1 \cdot 46 \pm 0 \cdot 63$) and ocean island basalt (OIB) ($20 \cdot 6$) (Table 2; Fig. 15) (Sun & McDonough, 1989; Kersting & Arculus, 1994; Ariskin *et al.*, 1995; Tatsumi *et al.*, 1995; Dorendorf *et al.*, 2000; Volynets *et al.*, 2000; Churikova *et al.*, 2001; Ishikawa *et al.*, 2001; Turner *et al.*, 2007). More specifically, Fig. 15b shows Gorely basalts (rear arc) in comparison with Mutnovsky (volcanic front) and Klyuchevskoy (Central Kamchatka Depression) basalts, in addition to basalts from Sunda, New Zealand, the New Hebrides, Java, and New Britain. Because the Central Kamchatka Depression magmas originate partially as a consequence of back-arc spreading, these provide a good comparison with magmas that are not fully sourced through subduction. As is shown in Fig. 15b, the Gorely basalts have compositions between those of OIB and other subduction-related mafic magmas around the world. Foundering of the lower crust could result in decompression melting of deeper, less depleted

mantle and thus magmas with more OIB-like compositions. In addition to the elevated Th relative to LREE observed by Duggen *et al.* (2007), we also observe high Nb, Zr, Ce, and P (Fig. 15b), which we suggest shows a smaller contribution of subduction fluids to the Gorely magmas, relative to volcanoes closer to the volcanic front, such as Mutnovsky. Therefore, we propose that Gorely magmas still carry a recognizable but subtle delamination component.

Glacial advances as a source for low-δ^{18}O magmas, and sporadic volcanic activity

As is shown in Fig. 16, the earliest ignimbrite-forming eruptions at Gorely, as well as the more recent ignimbrite eruptions at $\sim$38 ka, occur during glacial periods. Other recent ignimbrite eruptions in Kamchatka, from Odnoboky (from the Karymsky center), Ksudach, Uzon–Shorokoye, and Khangar (from the Sredinny Range) also erupted during maximal (75%) glacial periods (Fig. 16; Bindeman *et al.*, 2010). We include glacial length data (based on the moraine record) from Barr & Clark (2012) for Kamchatka in Fig. 16, because they proposed that glacial cycles in Kamchatka are offset from the average global glacial cycles. Even when using their data, which
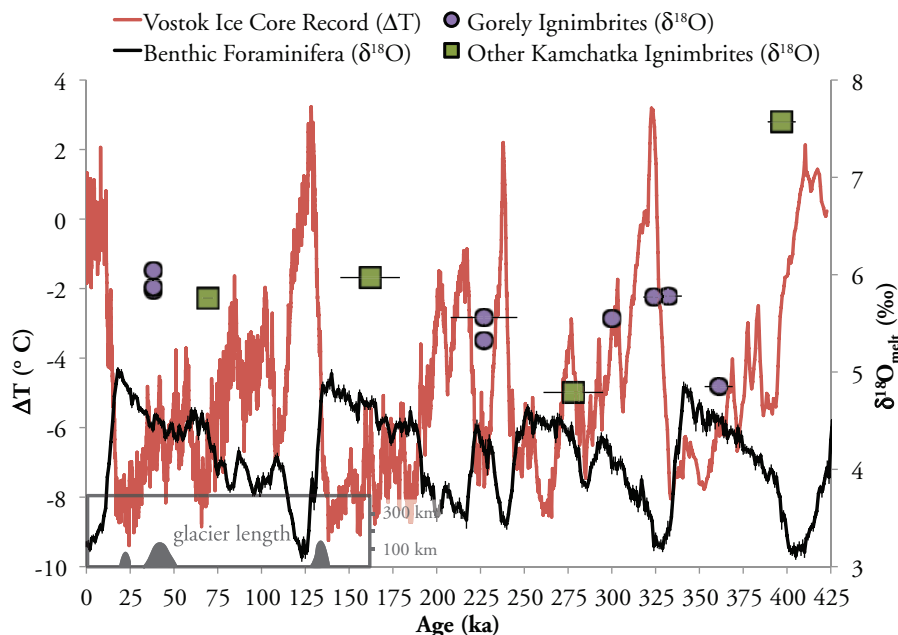

Fig. 16. Correlations between ages of newly dated, large ignimbrite-forming eruptions from Gorely volcano and global glacial cycles using the Vostok ice core and benthic foraminifera climate proxies. Glacier length in the Kamchatka Peninsula (Barr & Clark, 2012) is indicated in the lower left of the plot and represents the maximum length of the Kamchatkan glaciers during a specific time, which is sometimes offset from the global record. It should be noted that frequent ignimbrite eruptions (some with low δ^{18}O values) occur during maximal glacial conditions (high benthic foraminifera δ^{18}O and low Vostok ice ΔT), which is explained by frequent glacial erosion of the surface of the volcano, leading to decompression of the shallow magma chamber (e.g. Geyer & Bindeman, 2011). Gorely data with error bars are ^{40}Ar/^{39}Ar ages, and those without are correlated ages. Data from other Kamchatka ignimbrites include eruptions from Odnoboky, Ksudach, Uzon-Shorokoye, and Khangar (data from Bindeman *et al.*, 2010). Benthic foraminifera data are from Lisiecki & Raymo (2005); Vostok ice core data are from Jouzel *et al.* (1987, 1993, 1996), and Petit *et al.* (1999).

suggest fewer periods of glaciation in Kamchatka, our 38 ka ignimbrite eruptions still fall within a period of maximum glaciation. Although this is counter-intuitive to research that shows an increase in volcanism during shifts from glaciation to deglaciation (Tuffen, 2010), increases in volcanism during glacial periods have been shown to occur in Kamchatka, probably owing to glacial bulldozing effects and intrastadial sector collapses (Geyer & Bindeman, 2011). Additionally, we suggest that subglacial hydrothermal weakening (e.g. Merle et $al.$, 2010) could have further aided in the frequent late Pleistocene ignimbrite-forming eruptions at Gorely. The abundant low-$\delta^{18}O$ silicic volcanism in Kamchatka, and at Gorely in particular, serves as further confirmation of greater depletion of the magmas by lower $\delta^{18}O$ glacial meltwaters in Kamchatka as compared with North America or the Andes (Folkes et $al.$, 2013).

Repeated intracaldera glaciations in Gorely would allow for a low-$\delta^{18}O$ hydrothermal circulation system, which would create a sufficient supply of low-$\delta^{18}O$ rocks for assimilation into the Gorely magma system. At the same time, the surface action of glaciers could have created conditions for frequent ignimbrite eruptions from short-lived, variably $\delta^{18}O$ fingerprinted, ephemeral magma chambers (e.g. Geyer & Bindeman, 2011).

CONCLUSIONS

This study demonstrates considerable complexity in the evolution of a single, periodically glaciated, arc volcano. We have established a model of silicic magma generation at the Gorely eruptive center that involves periods of magmatic and hydrothermal activity spanning two of the most recent glacial cycles. Large-volume, isotopically distinct silicic magma can be generated incrementally at relatively shallow depths between more subdued phases of cone-building activity, and its generation is possibly enhanced through small-scale crustal foundering. Shallow depths of crustal assimilation and silicic magma generation are demonstrated in this study through three primary means: (1) MELTS modeling was not able to accurately reproduce the geochemical trends of the Gorely dacites, and could not even produce the trends of the Gorely basalts at pressures of 5 kbar; (2) the compositional gaps and isotopic variations are best explained by assimilation of the 11 Ma Akhomten Massif crust. Furthermore, (3) there is a limit to the depth of production of low-$\delta^{18}O$ magmas (Bindeman et $al.$, 2008). The production of large-volume, isotopically distinct, silicic magma occurs through a combination of fractional crystallization, melting of older and variably altered country rocks, and entrainment of cumulate crystal clusters. These silicic magma chambers are likely to empty nearly completely in ignimbrite eruptions after $10^3–10^5$ years of assembly, based on the frequency of ignimbrite eruptions and the

significant changes in isotopic composition. This study emphasizes the importance of analyzing these 'long-lived' volcanic centers with multiple geochemical tools, including geochronology, isotopes, major and trace element chemistry, mineral chemistry, and petrographic analysis, to determine their eruptive history. The use of just one of these tools would not reveal this long and detailed history of crustal foundering, crustal melting, crystal settling, mafic input, and eruption during alternating glaciations.

SUPPLEMENTARY DATA

Supplementary data for this paper are available at $Journal$ of $Petrology$ online.

REFERENCES

Annen, C., Blundy, J. D. & Sparks, R. S. (2006). The genesis of intermediate and silicic magmas in deep crustal hot zones. $Journal$ of $Petrology$ **47**, 505–539.

Ariskin, A. A., Barmina, G. S., Ozerov, A. & Nielsen, R. L. (1995). Genesis of high-alumina basalts from Klyuchevkoi volcano. $Petrology$ **3**, 449–472.

Asimow, P. D. & Ghiorso, M. S. (1998). Algorithmic modifications extending MELTS to calculate subsolidus phase relations. $American$ $Mineralogist$ **83**, 1127–1131.

Atherton, M. P. & Petford, N. (1993). Generation of sodium-rich magmas from newly underplated basaltic crust. $Nature$ **362**, 144–146.

Baboshina, V. A., Tereshchenkov, A. A. & Kharakhinov, V. V. (2000). Tectonic map of the sea of Okhotsk region. Russia: Institute of the Lithosphere of Marginal Seas, Russian Academy of Sciences, Scale 1:6,500,000, 1 sheet.

Balesta, S. T. (1991). Earth crust structure and magma chambers of the areas of present Kamchatka volcanism. In: Fedotov, S. A. & Masurenkov, Y. P. (eds) $Active$ $Volcanoes$ of $Kamchatka$. Nauka, pp. 36–45.

Barr, L. D. & Clark, C. D. (2012). Late Quaternary glaciations in far NE Russia; combining moraines, topography and chronology to

assess regional and global glaciation synchrony. *Quaternary Science Reviews* **53**, 72–87.

Basaltic Volcanism Study Project. (1981). *Basaltic Volcanism on the Terrestrial Planets*. Pergamon Press, 1286 p.

Bergantz, G. W. & Breidenthal, R. E. (2001). Non-stationary entrainment and tunneling eruptions: A dynamic link between eruption processes and magma mixing. *Geophysical Research Letters* **28**, 3075–3078.

Bindeman, I. (2008). Oxygen isotopes in mantle and crustal magmas as revealed by single crystal analysis. In: Putirka, K. D. & Tepley, F. J., III (eds) *Minerals, Inclusions and Volcanic Processes. Mineralogical Society of America and Geochemical Society, Reviews in Mineralogy and Geochemistry* **69**, 445–478.

Bindeman, I. N., Davis, A. & Drake, M. (1998). Ion microprobe study of plagioclase–basalt partition experiments at natural concentration levels of trace elements. *Geochimica et Cosmochimica Acta* **62**, 1175–1193.

Bindeman, I. N., Valley, J., Wooden, J. & Persing, H. (2001). Post-caldera volcanism: *in situ* measurement of U–Pb age and oxygen isotope ratio in Pleistocene zircons from Yellowstone caldera. *Earth and Planetary Science Letters* **189**, 197–206.

Bindeman, I. N., Vinogradov, V. I., Valley, J. W., Wooden, J. L. & Natal'in, B. A. (2002). Archean protolith and accretion of crust in Kamchatka: SHRIMP dating of zircons from Sredinny and Ganal Massifs. *Journal of Geology* **110**, 271–289.

Bindeman, I. N., Ponomareva, V., Bailey, J. & Valley, J. (2004). Volcanic arc of Kamchatka: A province with high $\delta^{18}O$ magma sources and large-scale $^{18}O/^{16}O$ depletion of the upper crust. *Geochimica et Cosmochimica Acta* **68**, 841–865.

Bindeman, I. N., Fu, B., Kita, N. T. & Valley, J. W. (2008). Origin and evolution of Yellowstone silicic magmatism based on ion microprobe analysis of isotopically zoned zircons. *Journal of Petrology* **49**, 163–193.

Bindeman, I. N., Leonov, V. L., Izbekov, P. E., Ponomareva, V. V., Watts, K. E., Shipley, N. K., Perepelov, A. B., Bazanova, L. I., Jicha, B. R., Singer, B. S., Schmitt, A. K., Portnyagin, M. V. & Chen, C. H. (2010). Large-volume silicic volcanism in Kamchatka: Ar–Ar and U–Pb ages, isotopic, and geochemical characteristics of major pre-Holocene caldera-forming eruptions. *Journal of Volcanology and Geothermal Research* **189**, 57–80.

Bohrson, W. A. & Spera, F. J. (2001). Energy-constrained open-system magmatic processes II: Application of energy-constrained assimilation–fractional crystallization (EC-AFC) model to magmatic systems. *Journal of Petrology* **42**, 1019–1041.

Braitseva, O. A., Melekestsev, I. V., Ponomareva, V. V. & Sulerzhisky, L. D. (1995). Ages of calderas, large explosive craters and active volcanoes in the Kuril–Kamchatka region, Russia. *Bulletin of Volcanology* **57**, 383–402.

Brophy, J. G. (1991). Composition gaps, critical crystallinity, and fractional crystallization in orogenic (calc-alkaline) magmatic systems. *Contributions to Mineralogy and Petrology* **109**, 173–182.

Chappell, B. W. & White, J. R. (2001). Two contrasting granite types: 25 years later. *Australian Journal of Earth Sciences* **48**, 489–499.

Chashchin, A. (1999). Ignimbrites of Gorely Volcano, southern Kamchatka: Composition and conditions of formation. *Trudy Dal'nevostochnogo Gosudarstvennogo Tekhnicheskogo Universiteta [in Russian]* **121**, 142–148.

Chashchin, A. A., Martynov, Yu. A., Perepelov, A. B., Ekimova, N. I. & Vladimirova, T. P. (2011). Physical and chemical conditions of the formation and evolution of Late Pleistocene-Holocene magmas of the Gorely and Mutnovsky Volcanoes, Southern Kamchatka. *Tikhookeanskaya Geologiya* **30**, 87–108.

Chayes, F. (1963). Relative abundance of intermediate members of the oceanic basalt–trachyte association. *Journal of Geophysical Research* **68**, 1519–1534.

Chiba, H., Chacko, T., Clayton, R. & Goldsmith, J. (1989). Oxygen isotope fractionations involving diopside, forsterite, magnetite, and calcite: Application to geothermometry. *Geochimica et Cosmochimica Acta* **53**, 2985–2995.

Christiansen, R. L. & Yeats, R. L. (1992). Post-Laramide geology of the U. S. Cordilleran region. In: Burchfiel, B. C., Lipman, P. W. & Zoback, M. L. (eds) *The Cordilleran Orogen: Conterminous US. Geological Society of America, Geology of America* **G-3**, 261–406.

Churikova, T. G., Dorendorf, F. & Barman, T. R. (2001). Sources and fluids in the mantle wedge below Kamchatka, evidence from across-arc geochemical variation. *Journal of Petrology* **42**, 1567–1593.

Czuppon, G., Lukács, R., Harangi, S., Mason, P. & Ntaflos, T. (2012). Mixing of crystal mushes and melts in the genesis of the Bogács Ignimbrite suite, northern Hungary: An integrated geochemical investigation of mineral phases and glasses. *Lithos* **148**, 71–85.

Daly, R. A. (1925). The geology of Ascension Island. *American Academy of Arts and Sciences Proceedings* **60**, 1–80.

Deering, C., Bachmann, O., Dufek, J. & Gravley, D. (2011). Rift-related transition from andesite to rhyolite volcanism in the Taupo Volcanic Zone (New Zealand) controlled by crystal–melt dynamics in mush zones with variable mineral assemblages. *Journal of Petrology* **52**, 2243–2263.

Deering, D., Vogel, T., Patino, L., Szymanski, D. & Alvarado, G. (2012). Magmatic processes that generate chemically distinct silicic magmas in NW Costa Rica and the evolution of juvenile continental crust in oceanic arcs. *Contributions to Mineralogy and Petrology* **163**, 259–275.

Dorendorf, F., Wiechert, U. H. & Wörner, G. (2000). Hydrated sub-arc mantle: A source for the Kluchevskoy volcano, Kamchatka/ Russia. *Earth and Planetary Science Letters* **175**, 69–86.

Druitt, T. H., Costa, F., Deloule, E. & Scaillet, B. (2012). Decadal to monthly timescales of magma transfer and reservoir growth at a caldera volcano. *Nature* **482**, 77–82.

Duggen, S., Portnyagin, M. V., Baker, J. A., Ulfbeck, D. G., Hoernle, K. A., Garbe-Schonber, D. & Grassineau, N. (2007). Drastic shift in lava geochemistry in the volcanic-front to rear-arc region of the southern Kamchatkan subduction zone: Evidence for the transition from slab surface dehydration to sediment melting. *Geochimica et Cosmochimica Acta* **71**, 452–480.

Dufek, J. & Bachmann, O. (2010). Quantum magmatism: Magmatic compositional gaps generated by melt-crystal dynamics. *Geology* **38**, 687–690.

Dufek, J. & Bergantz, G. W. (2005). Lower crustal magma genesis and preservation: A stochastic framework for the evaluation of basalt-crust interaction. *Journal of Petrology* **46**, 2167–2195.

Dungan, M. A. & Davidson, J. (2004). Partial assimilative recycling of the mafic plutonic roots of arc volcanoes: An example from the Chilean Andes. *Geology* **32**, 773–776.

Erlich, E. N. & Gorshkov, G. S. (1979). Quaternary volcanism and tectonics in Kamchatka. *Bulletin of Volcanology* **42**, 13–43.

Ewart, A. & Griffin, W. (1994). Application of proton-microprobe data to trace-element partitioning in volcanic rocks. *Chemical Geology* **117**, 251–284.

Folkes, C. B., de Silva, S. L., Bindeman, I. N. & Cas, R. (2013). Tectonic and climate history influence the geochemistry of large-volume silicic magmas: new $\delta^{18}O$ data from the Central Andes with comparison to N America and Kamchatka. *Journal of Volcanology and Geothermal Research* **262**, 90–102.

Gavrilenko, M. & Ozerov, A. (2010). Geochemical similarities between the pre-caldera and modern evolutionary series of eruptive products from Gorely volcano, Kamchatka. Abstract V21B-2333 presented at 2010 Fall Meeting, American Geophysical Union, Vol.1, p.2333.

Geyer, A. & Bindeman, I. (2011). Glacial influence on caldera-forming eruptions. *Journal of Volcanology and Geothermal Research* **202**, 127–142.

Ghiorso, M. & Sack, R. O. (1995). Chemical mass transfer in magmatic processes IV. A revised and internally consistent model for the interpolation and extrapolation of liquid–solid equilibria in magmatic systems at elevated temperatures and pressures. *Contributions to Mineralogy and Petrology* **119**, 197–212.

Gill, J. (1981). *Orogenic Andesites and Plate Tectonics*. New York: Springer.

Gorbatov, A., Kostoglodov, V., Suarez, G. & Gordeev, E. (1997). Seismicity and structure of the Kamchatka subduction zone. *Journal of Geophysical Research* **102**, 17883–17898.

Gorbatov, A., Domiguez, J., Suarez, G., Kostoglodov, V. & Gordeev, E. (1999). Tomographic imaging of the P-wave velocity structure beneath the Kamchatka peninsula. *Journal of Geophysical Research* **137**, 269–279.

Gordeev, E. I., Gusev, A. A., Levin, V. E., Bakhtiarov, V. F., Pavlov, V. M., Chebrov, V. N. & Kasahara, M. (2001). Preliminary analysis of deformation at the Eurasia–Pacific–North America plate junction from GPS data. *Geophysical Journal International* **147**, 189–198.

Grove, T. L. & Donnelly-Nolan, J. M. (1986). The evolution of young silicic lavas at Medicine Lake Volcano, California: Implications for the origin of compositional gaps in calc-alkaline series lavas. *Contributions to Mineralogy and Petrology* **92**, 281–302.

Grove, T. L. & Kinzler, R. J. (1986). Petrogenesis of andesites. *Annual Review of Earth and Planetary Sciences* **14**, 417–454.

Grove, T. L., Donnelly-Nolan, J. M. & Housh, T. (1997). Magmatic processes that generated the rhyolite of Glass Mountain, Medicine Lake volcano, N. California. *Contributions to Mineralogy and Petrology* **127**, 205–223.

Grove, T. L., Parman, S. W., Bowring, S. A., Price, R. C. & Baker, M. B. (2002). The role of an H_2O-rich fluid component in the generation of primitive basaltic andesites and andesites from Mt. Shasta region, N California. *Contributions to Mineralogy and Petrology* **142**, 375–396.

Grove, T. L., Elkins-Tanton, L. T., Parman, S. W., Chatterjee, N., Müntener, O. & Gaetani, G. A. (2003). Fractional crystallisation and mantle-melting controls on calc-alkaline differentiation trends. *Contributions to Mineralogy and Petrology* **145**, 515–533.

Heath, E., Turner, S. P., Macdonald, R., Hawkesworth, C. J. & van Calsteren, P. (1998). Long magma residence times at an island arc volcano (Soufriere, St. Vincent) in the Lesser Antilles: Evidence from 238U230Th isochron dating. *Earth and Planetary Science Letters* **160**, 49–63.

Hedge, C. E. & Gorshkov, G. S. (1977). Strontium-isotope composition of volcanic rocks from Kamchatka. *Doklady Akademiya Nauk SSSR* **233**, 163–166.

Hildreth, W. & Moorbath, S. (1988). Crustal contribution to arc magmatism in the Andes of Central Chile. *Contributions to Mineralogy and Petrology* **98**, 455–489.

Hochstaedter, A., Gill, J., Peters, R., Broughton, P. & Holden, P. (2001). Across-arc geochemical trends in the Izu–Bonin arc: Contributions from the subducting slab. *Geochemistry, Geophysics, Geosystems* **2**, Paper number 2000GC000105.

Hochstaedter, A. G., Kepezhinskas, P. K. & Defant, M. J. (1996). Insights into the volcanic arc mantle wedge from magnesian lavas from the Kamchatka Arc. *Journal of Geophysical Research* **B101**, 697–712.

Hourigan, K., Brandon, M. T., Soloviev, A. V., Kirmasov, A. B., Garver, J. I. & Reiners, P. W. (2009). Eocene arc–continent collision and crustal consolidation in Kamchatka, Russian Far East. *American Journal of Science* **309**, 333–396.

Hughes, G. & Mahood, G. A. (2008). Tectonic controls on the nature of large silicic calderas in volcanic arcs. *Geology* **36**, 627–630.

Humphreys, E. (1995). Post-Laramide removal of the Farallon slab, western United States. *Geology* **23**, 987–990.

Ishikawa, T. & Tera, F. (1997). Source, composition and distribution of the fluid in the Kurile mantle wedge: Constraints from across-arc variations of B/Nb and B isotopes. *Earth and Planetary Science Letters* **152**, 123–138.

Ishikawa, T., Tera, F. & Nakazawa, T. (2001). Boron isotope and trace element systematics of the three volcanic zones in the Kamchatka arc. *Geochimica et Cosmochimica Acta* **65**, 4523–4537.

Izbekov, P., Eichelberger, J. & Ivanov, B. (2004a). The 1996 eruption of Karymsky volcano, Kamchatka: Historical record of basaltic replenishment of an andesite reservoir. *Journal of Petrology* **45**, 2325–2345.

Izbekov, P., Gardner, J. E. & Eichelberger, J. C. (2004b). Comagmatic granophyre and dacite from Karymsky volcanic center, Kamchatka; Experimental constraints and magma storage conditions. *Journal of Volcanology and Geothermal Research* **131**, 1–18.

Jicha, B. R., Rhodes, J. M., Singer, B. S. & Carcia, M. O. (2012). $^{40}Ar/^{39}Ar$ geochronology of submarine Mauna Loa volcano, Hawaii. *Journal of Geophysical Research* **117**, B09204.

John, D. A., Sisson, T. W., Breit, G. N., Rye, R. O. & Vallance, J. W. (2008). Characteristics, extent and origin of hydrothermal alteration at Mount Rainier Volcano, Cascades Arc, USA: Implications for debris-flow hazards and mineral deposits. *Journal of Volcanology and Geothermal Research* **175**, 289–314.

Johnson, D. M., Hooper, P. R. & Conrey, R. M. (1999). XRF analysis of rocks and minerals for major and trace elements on a single low dilution Li-tetraborate fused bead. *Advances in X-ray Analysis* **41**, 843–867.

Jouzel, J., Lorius, C., Petit, J. R., Genthon, C., Barkov, N. I., Kotlyakov, V. M. & Petrov, V. M. (1987). Vostok ice core: a continuous isotope temperature record over the last climatic cycle (160,000 years). *Nature* **329**, 403–408.

Jouzel, J., Barkov, N. I., Barnola, J. M., Bender, M., Chappellaz, J., Genthon, C., Kotlyakov, V. M., Lipenkov, V., Lorius, C., Petit, J. R., Raynaud, D., Raisbeck, G., Ritz, C., Sowers, T., Stievenard, M., Yiou, F. & Yiou, P. (1993). Extending the Vostok ice-core record of palaeoclimate to the penultimate glacial period. *Nature* **364**, 407–412.

Jouzel, J., Waelbroeck, C., Malaize, B., Bender, M., Petit, J. R., Stievenard, M., Barkov, N. I., Barnola, J. M., King, T., Kotlyakov, V. M., Lipenkov, V., Lorius, C., Raynaud, D., Ritz, C. & Sowers, T. (1996). Climatic interpretation of the recently extended Vostok ice records. *Climate Dynamics* **12**, 513–521.

Kepezhinskas, P. K., McDermott, F., Defant, M., Hochstaedter, A. G., Drummond, M. S., Hawkesworth, C. J., Koloskov, A. V., Maury, R. C. & Bellon, H. (1997). Trace element and Sr–Nd–Pb isotopic constraints on a three-component model of Kamchatka Arc petrogenesis. *Geochimica et Cosmochimica Acta* **61**, 577–600.

Kersting, A. B. & Arculus, R. J. (1994). Kamchatka, Russia: The role of high-flux recharged, trapped, and fractionated magma chamber(s) in the genesis of high-Al_2O_3 from high-MgO basalt. *Journal of Petrology* **35**, 1–41.

Kirsanov, I. T. & Melekestsev, I. V. (1991). Gorely Volcano. In: Fedotov, S. A. (ed.) *Active Volcanoes of Kamchatka 2.* Nauka, pp. 294–315.

Konstantinovskaya, E. A. (2003). Margins of the east seas: tectonics, structural evolution and geodynamic modeling. *Moscow: Scientific World* **549**, 224 (in Russian).

Kraus, J. U. & Scotese, C. R. (1993). , Global polygon and suture map. Department of Geology, University of Texas at Arlington, Texas, Paleomap Progress Report 19–0293, p. 12.

Kuiper, K. F., Deino, A., Hilgen, F. J., Krijgsman, W., Renne, P. R. & Wijbrans, J. R. (2008). Synchronizing rock clocks of Earth history. *Science* **320**, 500–504.

Lander, A. & Shapiro, M. (2007). The origin of the modern Kamchatka subduction zone. In: Eichelberger, J., Gordeev, E., Kasahara, M., Izbekov, P. & Lees, J. (eds) *Volcanism and Subduction: The Kamchatka Region. American Geophysical Union, Geophysical Monograph* **172**, 57–64.

Lisiecki, L. E. & Raymo, M. E. (2005). A Pliocene–Pleistocene stack of 57 globally distributed benthic δ^{18}O records. *Paleoceanography* **20**, PA1003.

Marsh, B. D. (1981). On the crystallinity, probability of occurrence, and rheology of lava and magma. *Contributions to Mineralogy and Petrology* **78**, 85–98.

Melekhova, E., Annen, C. & Blundy, J. (2013). Compositional gaps in igneous rock suites controlled by magma system heat and water content. *Nature Geoscience* **6**, 285–390.

Merle, O., Barde-Cabusson, S. & de Vries, B. (2010). Hydrothermal calderas. *Bulletin of Volcanology* **72**, 131–147.

Min, K., Mundil, R., Renne, P. & Ludwig, K. (2000). A test for systematic errors in ^{40}Ar/^{39}Ar geochronology through comparison with U/Pb analysis of a 1·1-Ga rhyolite. *Geochimica et Cosmochimica Acta* **64**, 73–98.

Müntener, O., Kelemen, P. B. & Grove, T. L. (2001). The role of H_2O during crystallisation of primitive arc magmas under uppermost mantle conditions and genesis of igneous pyroxenites: An experimental study. *Contributions to Mineralogy and Petrology* **141**, 643–658.

Musselwhite, D. S., De Paolo, D. J. & McCurry, M. (1989). The evolution of a silicic magma system—isotopic and chemical evidence from the Woods Mountains Volcanic Center, Eastern California. *Contributions to Mineralogy and Petrology* **101**, 19–29.

Nagasawa, H. & Schnetzler, C. (1971). Partitioning of rare earth, alkali, and alkaline earth elements between phenocrysts and acidic igneous magmas. *Geochimica et Cosmochimica Acta* **35**, 953–968.

Onuma, N., Higuchi, H., Wakita, H. & Nagasawa, H. (1968). Trace element partition between two pyroxenes and the host lava. *Earth and Planetary Science Letters* **5**, 47–51.

Ozerov, A. Yu., Ariskin, A. A. & Barmina, G. S. (1995). The problem of genetic relations between high-alumina basalts and high-magnesian basalts of the Klyuchevskoi Volcano, Kamchatka (Trans.). *Doklady Acadamy of Sciences USSR* **350**, 1127–1130.

Petford, N. & Atherton, M. (1996). Na-rich partial melts from newly underplated basaltic crust: The Cordillera Blanca Batholith, Peru. *Journal of Petrology* **37**, 1491–1521.

Petit, J. R., Jouzel, J., Raynaud, D., Barkov, N. I., Barnola, J. M., Basile, I., Bender, M., Chappellaz, J., Davis, M., Delayque, G., Delmotte, M., Kotlyakov, V. M., Legrand, M., Lipenkov, V. Y., Lorius, C., Pepin, L., Ritz, C., Saltzman, E. & Stievenard, M. (1999). Climate and atmospheric history of the past 420,000 years from the Vostok ice core, Antarctica. *Nature* **399**, 429–436.

Pineau, F., Semet, M. P., Grassineau, N., Okrugin, V. M. & Javoy, M. (1999). The genesis of stable isotope (O, H) record in arc magmas: The Kamchatkan Case. *Chemical Geology* **153**, 93–124.

Ponomareva, V., Melekestsev, I., Braitseva, O., Churikova, T., Pevzner, M. & Sulerzhitsky, L. (2007). Late Pleistocene–Holocene volcanism on the Kamchatka Peninsula, Northwest Pacific Region. In: Eichelberger, J., Gordeev, E., Kasahara, M., Izbekov, P. & Lees, J. (eds) *Volcanism and Subduction: The Kamchatka Region. American Geophysical Union, Geophysical Monograph* **172**, 165–198.

Poplitov, E. I. & Volynets, O. N. (1981). *Geochemical Characteristics of Quaternary Volcanism of the Kurile–Kamchatka Island Arc.* Moscow: Nauka (in Russian).

Putirka, K. D. (2008). Thermometers and barometers for volcanic systems. In: Putirka, K. D. & Tepley, F. J., III (eds) *Minerals, Inclusions and Volcanic Processes. Mineralogical Society of America and Geochemical Society, Reviews in Mineralogy and Geochemistry* **69**, 61–120.

Rapp, R. P. & Watson, E. B. (1995). Dehydration melting of metabasalt at 8–32 kbar: Implications for continental growth and crust–mantle recycling. *Journal of Petrology* **36**, 891–931.

Reubi, O. & Blundy, J. (2009). A dearth of intermediate melts at subduction zone volcanoes and the petrogenesis of arc andesites. *Nature* **461**, 1269–1273.

Rogers, G. & Hawkesworth, C. J. (1989). A geochemical traverse across the North Chilean Andes: Evidence for crust generation from the mantle wedge. *Earth and Planetary Science Letters* **91**, 271–285.

Rubatto, D. (2002). Zircon trace element geochemistry: Partitioning with garnet and the link between U–Pb ages and metamorphism. *Chemical Geology* **184**, 123–138.

Rudnick, R. L. & Fountain, D. M. (1995). Nature and composition of the continental crust: A lower crustal perspective. *Reviews of Geophysics* **33**, 267–309.

Scholl, D. (2007). Viewing the tectonic evolution of the Kamchatka–Aleutian (KAT) connection with an Alaska crustal extrusion perspective. In: Eichelberger, J., Gordeev, E., Kasahara, M., Izbekov, P. & Lees, J. (eds) *Volcanism and Subduction: The Kamchatka Region. American Geophysical Union, Geophysical Monograph* **172**, 3–35.

Selyangin, O. (2006). *The Wonderful World of Mutnovsky and Gorely Volcanoes: A Guide for Volcanologists and Travelers, Petropavlovsk-Kamchatsky.*

Selyangin, O. & Ponomareva, V. (1999). Structure and evolution of the Gorelovsky volcanic center, southern Kamchatka. *Volcanology and Seismology* **1**, 3–23.

Sheimovich, V. S. & Karpenko, M. I. (1996). K–Ar volcanism of Southern Kamchatka. *Volcanology and Seismology* **18**, 86–90.

Shipley, N. K. (2011). Isotopic and petrologic investigation and model of genesis of large-volume high-silica rhyolites in arc environments: Karymshina caldera, Kamchatka, Russia. MA thesis, University of Oregon, Eugene, 76 pp.

Siebert, L. & Simkin, T. (2002). *Volcanoes of the World: An Illustrated Catalog of Holocene Volcanoes and their Eruptions.* Smithsonian Institution, Global Volcanism Program, Digital Information Series.

Simakin, A. & Bindeman, I. N. (2012). Remelting in caldera and rift environments and the genesis of hot, 'recycled' rhyolites. *Earth and Planetary Science Letters* **337–338**, 224–235.

Smith, D. R. & Leeman, W. P. (1987). Petrogenesis of Mount St. Helens dacitic magmas. *Journal of Geophysical Research* **92**, 10313–10334.

Soloviev, A. V., Shapiro, M. N. & Garver, J. I. (2002a). Lesnaya nappe, northern Kamchatka. *Geotectonics* **36**, 469–482.

Soloviev, A. V., Shapiro, M. N., Garver, J. I., Shcherbinina, E. A. & Kravchenko-Berezhnoy, I. R. (2002b). New age data from the Lesnaya Group: A key to understanding the timing of arc–continent collision, Kamchatka, Russia. *Island Arc* **11**, 79–90.

Sparks, R. & Marshall, L. (1986). Thermal and mechanical constraints on mixing between mafic and silicic magmas. *Journal of Volcanology and Geothermal Research* **29**, 99–124.

Spera, F. J. & Bohrson, W. A. (2001). Energy-constrained open-system magmatic processes I: General model and energy-constrained assimilation and fractionation crystallization (EC-AFC) formulation. *Journal of Petrology* **42**, 999–1018.

Steiger, R. H. & Jäger, E. (1977). Subcommission on geochronology: Convention on the use of decay constants in geo- and cosmochronology. *Earth and Planetary Science Letters* **36**, 359–362.

Sun, S. S. & McDonough, W. F. (1989). Chemical and isotopic systematics of oceanic basalts: Implications for mantle composition and processes. In: Saunders, A. D. & Norry, M. J. (eds) *Magmatism in the Ocean Basins. Geological Society, London, Special Publications* **42**, 313–345.

Tatsumi, Y., Kogiso, T. & Nohda, S. (1995). Formation of a third volcanic chain in Kamchatka: Generation of unusual subduction-related magmas. *Contributions to Mineralogy and Petrology* **120**, 117–128.

Taylor, R. N. & Nesbitt, R. W. (1998). Isotopic characteristics of subduction fluids in an intra-oceanic setting, Izu–Bonin Arc, Japan. *Earth and Planetary Science Letters* **164**, 79–98.

Tepper, J. H., Nelson, B. K., Bergantz, G. W. & Irving, A. J. (1993). Petrology of the Chiilwack batholith, North Cascades, Washington. Generation of calc-alkaline granitoids by melting of mafic lower crust with variable water fugacity. *Contributions to Mineralogy and Petrology* **113**, 333–351.

Thompson, A. B., Matile, L. & Ulmer, P. (2002). Some thermal constraints on crustal assimilation during fractionation of hydrous, mantle-derived magmas with examples from central Alpine batholiths. *Journal of Petrology* **43**, 403–422.

Tollan, P., Bindeman, I. & Blundy, J. (2012). Cumulate xenoliths from St. Vincent, Lesser Antilles Island Arc: a window into upper crustal differentiation of mantle-derived basalts. *Contributions to Mineralogy and Petrology* **163**, 189–208.

Tolstykh, M. L., Naumov, V. B., Gavrilenko, M. G., Ozerov, A. Y. & Kononkova, N. N. (2012). Chemical composition, volatile components, and trace elements in the melts of the Gorely Volcanic Center, southern Kamchatka: Evidence from inclusions in minerals. *Geochemistry International* **50**, 522–550.

Tuffen, H. (2010). How will melting of ice affect volcanic hazards in the twenty-first century? *Philosophical Transactions of the Royal Society of London, Series A* **368**, 2535–2558.

Turner, S. P., Sims, K. W. W., Reagan, M. K. & Cook, C. (2007). A $^{210}Pb–^{226}Ra–^{230}Th–^{238}U$ study of Klyuchevskoy and Bezymianny volcanoes, Kamchatka. *Geochimica et Cosmochimica Acta* **71**, 4771–4785.

Vinogradov, V. I. (1995). Isotopic evidence of the conversion of oceanic crust to continental crust in the continent–ocean transition zone of Kamchatka. *Geochemistry International* **32**, 70–109.

Vinogradov, V. I. & Vakin, Y. (1983). Strontium isotopes of the thermal waters of Kamchatka (Trans.). *Doklady Acadamy of Sciences USSR* **273**, 965–968.

Volynets, O. N., Babanskii, A. D. & Gol'tsman, Y. (2000). Variations in isotopic and trace-element composition of lavas from volcanoes of the northern group, Kamchatka, in relation to specific features of subduction. *Geochemistry International* **38**, 974–989.

Walker, J. A., Carr, M. J., Patino, L. C., Johnson, C. M., Feigenson, M. D. & Ward, R. L. (1995). Abrupt change in magma generation processes across the Central American arc in southeastern Guatemala: Flux-dominated melting near the base of the wedge to decompression melting near the top of the wedge. *Contributions to Mineralogy and Petrology* **120**, 378–390.

Weismaier, S., Troll, V., Carracedo, J., Ellam, R., Bindeman, I. & Wolff, J. (2012). Bimodality of lavas in the Teide–Pico Viejo succession in Tenerife—the role of crustal melting in the origin of recent phonolites. *Journal of Petrology* **53**, 2465–2495.